AD-A165 217 ASSESSMENT OF METHODS FOR MONITORING THE IONOSPHERE BY OBSERVING UV AND V... (U) BEERS ASSOCIATES INC RESTON VA R E DANIELL ET AL. JAN 85 AFGL-TR-85-0013 1/1

UNCLASSIFIED F19628-83-C-0078 F/G 4/1 NL

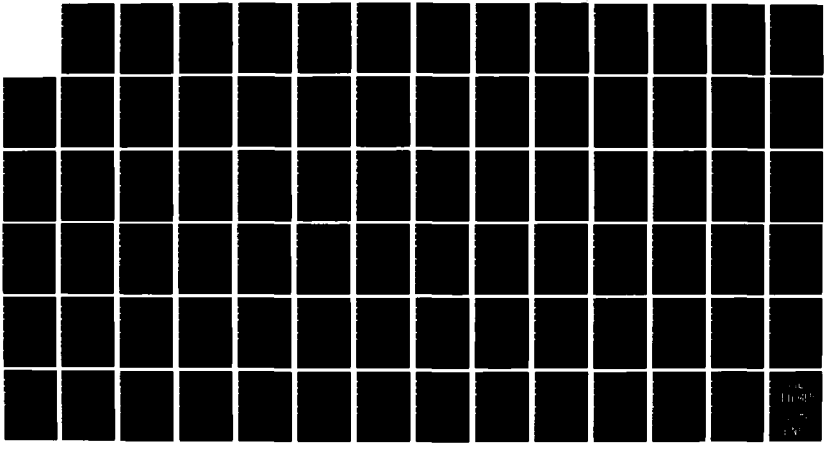

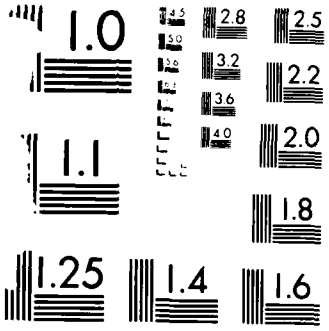

AFGL-TR-85-0013

ASSESSMENT OF METHODS FOR MONITORING THE IONOSPHERE BY OBSERVING UV AND VISIBLE EMISSIONS

R. E. Daniell, Jr.
D. J. Strickland

Beers Associates, Inc
P.O. Box 2549
Reston, VA 22090

January 1985

Final Report
23 February 1983 - 30 June 1984

AIR FORCE GEOPHYSICS LABORATORY
AIR FORCE SYSTEMS COMMAND
UNITED STATES AIR FORCE
HANSCOM AIR FORCE BASE, MASSACHUSETTS 01731

"This technical report has been reviewed and is approved for publication"

MILTON M. KLEIN
Contract Manager
Ionospheric Effects Branch

HERBERT C. CARLSON, Chief
Ionospheric Effects Branch
Ionospheric Physics Division

FOR THE COMMANDER

ROBERT A. SKRIVANEK
Director
Ionospheric Physics Division

This report has been reviewed by the ESD Public Affairs Office (PA) and is releasable to the National Technical Information Service (NTIS).

Qualified requestors may obtain additional copies from the Defense Technical Information Center. All others should apply to the National Technical Information Service.

If your address has changed, or if you wish to be removed from the mailing list, or if the addressee is no longer employed by your organization, please notify AFGL/DAA, Hanscom AFB, MA 01731. This will assist us in maintaining a current mailing list.

UNCLASSIFIED

SECURITY CLASSIFICATION OF THIS PAGE

REPORT DOCUMENTATION PAGE

1a. REPORT SECURITY CLASSIFICATION Unclassified	1b. RESTRICTIVE MARKINGS None
2a. SECURITY CLASSIFICATION AUTHORITY N/A	3. DISTRIBUTION/AVAILABILITY OF REPORT Approved for public release; distribution unlimited
2b. DECLASSIFICATION/DOWNGRADING SCHEDULE	
4. PERFORMING ORGANIZATION REPORT NUMBER(S)	5. MONITORING ORGANIZATION REPORT NUMBER(S) AFGL-TR-85-0013
6a. NAME OF PERFORMING ORGANIZATION Beers Associates, Inc. — 6b. OFFICE SYMBOL (If applicable)	7a. NAME OF MONITORING ORGANIZATION Air Force Geophysics Laboratory
6c. ADDRESS (City, State and ZIP Code) P.O. Box 2549 Reston, VA 22090	7b. ADDRESS (City, State and ZIP Code) Hanscom AFB Bedford, MA 01731
8a. NAME OF FUNDING/SPONSORING ORGANIZATION Air Force Geophysics Laboratory — 8b. OFFICE SYMBOL (If applicable) LIS	9. PROCUREMENT INSTRUMENT IDENTIFICATION NUMBER F19628-83-C-0078
8c. ADDRESS (City, State and ZIP Code) Hanscom AFB MA 01731	10. SOURCE OF FUNDING NOS. PROGRAM ELEMENT NO. 62101F — PROJECT NO. 4643 — TASK NO. 07 — WORK UNIT NO. AB
11. TITLE (Include Security Classification) Assessment of Methods for Monitoring the Ionosphere by Observing UV and Visible Emissions	
12. PERSONAL AUTHOR(S) Daniell, R.E., Jr., and Strickland, D.J.	
13a. TYPE OF REPORT Final	13b. TIME COVERED FROM 2-23-83 TO 6-30-84
14. DATE OF REPORT (Yr., Mo., Day) 1985 January	15. PAGE COUNT 86
16. SUPPLEMENTARY NOTATION	

17 COSATI CODES		
FIELD	GROUP	SUB. GR.
04	01	
20	09	

18. SUBJECT TERMS (Continue on reverse if necessary and identify by block number)
Optical Emissions; Satellite Measurements; UV Sensors; Electron Density; Photometer; Rocket Measurements; EUV Emissions; Spectrometer; Dayglow; Nightglow; Photoelectron Flux

19. ABSTRACT (Continue on reverse if necessary and identify by block number)

Two nighttime codes have been developed for obtaining the electron density profile in the lower to midlatitude ionosphere by using optical emission of oxygen 6300A and 1356A. The nighttime background present in the bandpass of a 6300A photometer was investigated. It was found that a 2A tilting filter photometer should be able to determine the true intensity of the oxygen 6300A line within reasonable integration time constraints. A code was developed which determines limb intensity profiles for optically thick or thin emissions with or without pure absorption. The method is efficient and highly accurate. An analysis has been made of the data from a dayglow rocket experiment, UV intensities measured on board a sounding rocket, and ground based ionosonde data. The electron density profile and the UV intensities obtained from the data were compared with corresponding results predicted by codes developed herein. It was found that the calculations could not reproduce both the electron density profile and the optical data, the discrepancy being most pronounced at the lower altitudes.

20 DISTRIBUTION/AVAILABILITY OF ABSTRACT UNCLASSIFIED/UNLIMITED ☐ SAME AS RPT. ☒ DTIC USERS ☐	21 ABSTRACT SECURITY CLASSIFICATION Unclassified
22a NAME OF RESPONSIBLE INDIVIDUAL Milton M. Klein	22b TELEPHONE NUMBER (Include Area Code) 617-861-3137 — 22c OFFICE SYMBOL AFGL/LIS

DD FORM 1473, 83 APR — EDITION OF 1 JAN 73 IS OBSOLETE.

Unclassified

SECURITY CLASSIFICATION OF THIS PAGE

TABLE OF CONTENTS

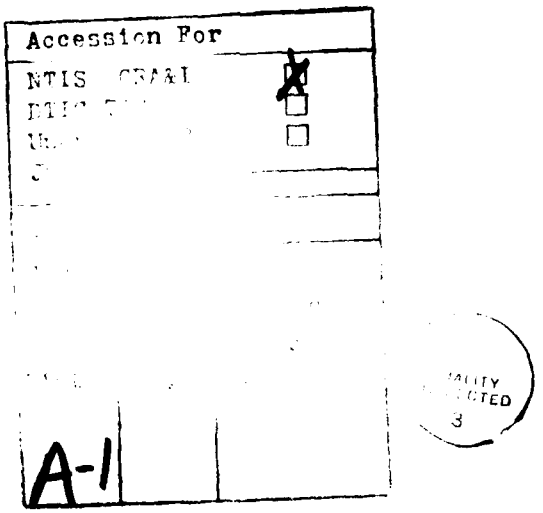

1. Introduction and Summary

This report documents work performed for the Air Force Geophysics Laboratory (AFGL) and the Air Force Space Division (AFSD) on the subject of optical emissions from the ionosphere and their relationship to electron density profiles (EDPs). The work spans the period from February 1983 to September 1984, with actual completion several months prior to the termination date. Considerable documentation was produced under this contract:

- Quarterly reports (6/83, 9/83, 12/83, and 3/84)
- Technical report to AFSD (Strickland et al., 1984a)
- This final report
- Publications
  - Strickland et al. (1984b)
  - Daniell et al. (1984)
  - Daniell and Strickland (1985).

Copies of the publications appear as appendices to this report.

Prior contract work concentrated on the study of auroral processes using first-principles models and applying these to making predictions and analyzing rocket and satellite data. Interest focussed on the continuous aurora to better understand chemical and radiation processes and determine how useful satellite optical data can be in deducing the auroral E EDP (see Strickland et al., 1983a). Work during the present contract expanded to include investigation of ionospheric processes in the mid-latitude nighttime and low to mid-latitude daytime ionospheres. Much of our time was directed to the nighttime problem which is briefly outlined in the next section, and has been documented in the above referenced AFSD report and in the paper by Daniell et al. (1984). We have determined in quantitative terms how well one can expect to deduce the nighttime EDP under quiescent plasma conditions from the weak atomic

oxygen emissions resulting from recombination of O_2^+ and O^+ with ambient electrons. Present state-of-the-art detectors recording data from a satellite such as DMSP will significantly improve the Air Force's present near real-time specification of this EDP.

We may summarize our progress and findings as follows:

1. Two nighttime codes have been developed and applied. One specifies the nighttime EDP given nadir intensities of OI 6300 and OI 1356 A. The other does the reverse calculation. Both codes use an empirical (Chapman) model to characterize the shape of the EDP.

2. A literature survey of emissions and the EDP under the nighttime conditions was conducted. The survey, plus application of the above codes, have provided good morphological information on these quantities, giving their behavior as functions of local time, season, solar activity, and latitude.

3. The nighttime background to be found in the bandpass of a 6300 A photometer was investigated. Its contribution to the 6300 A signal was determined for various tilting filter configurations and over the full range of lunar luminosities. It was determined that a 2A tilting filter photometer should be able to effectively determine the true OI 6300 A intensity within integration time constraints.

4. An investigation was carried out which provided instrument specifications needed to adaquately measure optical intensities at night, in the day, and for the continuous aurora. The specifications for day and auroral observations applied to a spectrometer while those for nighttime observations applied to photometers. Section 4 reports our findings.

5. An investigation of auroral EUV emissions was conducted to determine their variability and possible use in deducing EDPs (Strickland et al., 1983b). This was documented in the second quarterly report.

6. A code was developed which determines limb intensity profiles for optically thick or thin emissions with or without pure absorption. The algorithim is efficient and guarantees a high degree of accuracy since the integrand is investigated prior to integration. This is documented in the first quarterly report.

7. Modeling of the daytime EDP and selected optical emissions was conducted to compare with rocket and ground-based sounder data and with independent modeling results being obtained at AFGL by Decker and Jasperse. See Section 5 for a discussion of the daytime problem.

8. Further analysis was carried out on the optical and EDP data from the AFGL auroral E rocket program. Good agreement was achieved with the available data. Details are available in Section 5 of the AFSD report. Publication of the analysis is planned in 1985.

9. An ongoing search was performed for experiments (rocket, satellite, and ground based) yielding simultaneous EDP and optical data in the three global regions cited above. The most notable example found is discussed in Section 5.

In summary, several investigations were conducted with emphasis on determining how well optical data can be used to deduce the EDP in the nighttime, daytime, and auroral ionospheres. The problem was limited to the E region in the case of the aurora. Both the E and F regions were of interest for the other two regions. We have much better quantitative information on the use of this concept than when this work began. It looks particularly attractive at night where the emissions provide a direct signature of the EDP. Much more work is still needed, especially with regard to F region global behavior.

A satellite experiment is also needed to definitively test our models being used to relate optical intensities to EDPs. Such an experiment will probably begin in 1989 under the direction of Meier and colleagues at the Naval Research Laboratory. The instrument is called RAIDS (Remote

Atmospheric and Ionospheric Detection System). It will measure intensities from the EUV to the visible for various viewing geometries (including nadir and limb viewing). Simultaneous EDP measurements will occur when the satellite is passing over ground-based ionosonde stations. Huffman and colleagues at AFGL are also beginning work on an operational system to fly on DMSP in the late 1980s and early 1990s. This is the system for which we have been conducting feasibility studies over the pase several years. Nadir observed intensities and in situ measurements of the electron density and temperature are being planned with simultaneous measurements of the EDP by ground-based ionosondes whenever DMSP is approximately overhead. The RAIDS experiment, which is research oriented, should provide valuable information to us prior to the start of Huffman's operational system.

2. Overview

We have included this section to address the following items:

- Larger Air Force interests
- Categories under which the completed work may be broken down
- Documentation in this report versus total documentation under this contract

This work is motivated by the need to improve the present near real time specification of the EDP on a global scale from the lower E region to the upper F region. Systems in need of this information include HF communications systems, over-the-horizon (OTH) radar systems, SPACETRACK radar systems, and classified systems. Satellites are the measuring platforms needed for global coverage and offer two options for monitoring the EDP: active or remote sensing. Active sensing requires the use of an ionosonde which yields the EDP maximum. Passive sensing requires the use of photometers and/or spectrometers capable of measuring radiations over a wide intensity range. These intensities can be related to EDP characteristics as well as the dominant neutral densities. The key issue here relates to the size of error bars placed on the deduced EDP and whether it is small enough to significantly improve present global EDP specification.

We have been investigating the passive sensing problem for the past few years. Prior to this contract, work concentrated primarily on the aurora - in particular, the continuous aurora known for its stability over tens of minutes (see, e.g., Whalen, 1981). Good examples of studies undertaken may be seen in the papers by Strickland et al. (1983a) and Daniell and Strickland (1985). We have examined in detail how a variety of emissions from the EUV to the visible along with the EDP change as functions of the precipitating electron spectrum and atmospheric conditions. We found that selected emission efficiencies changed noticeably, showing potential for monitoring electron precipitation characteristics which in turn can yield the EDP through modeling. This work concentrated on EDP specification for the E region.

In this contract, emphasis has shifted from the auroral ionosphere to the mid-latitude nighttime and daytime ionospheres. Part of this was caused by the discovery of strong clutter in OTH returns from the auroral ionosphere during radar experiments conducted by the Air Force. The clutter is produced by plasma structure arising from instabilities and reduces the potential of OTH radar as an effective tool for detecting aircraft and missiles at high northern latitudes. Beyond this, there was a need to begin examining the optical concept elsewhere since interest is on a global scale. As noted in the introduction, most of our effort has been directed to the nighttime ionosphere. Some work has continued on auroral problems, particularly on analysis of data from the AFGL auroral E rocket program. Some work has also been carried out on the daytime problem, mainly in collaboration with AFGL personnel.

Table 1 shows a breakdown into eight categories of the work undertaken in this contract. We see that most catagories apply to the nighttime investigation. A brief description of this investigation follows. We began by developing two codes which relate the OI 6300 A and OI 1356 A emissions (there are other OI lines such as 1304 A which could serve the same purpose as 1356 A) to the EDP. One code calculated an EDP (assuming a Chapman dependence) from the emissions while the other does the reverse calculation given a particular EDP. These codes were used to predict the morphological behavior of these emissions and to examine the sensitivity of the EDP to variaions in either emission. Another important aspect of the work was to characterize the background around OI 6300 A and do statistical studies to determine how long this feature must be observed to extract a good 6300 A signal. The assumed detection system was a tilting filter photometer with various bandpasses. Such a photometer is capable of scanning in wavelength, which enables the true signal to be separated from the background signal. Detectability was investigated for various levels of background and OI 6300 A intensity. The most detailed documentation of the nighttime investigation appears in our recent AFSD report (Strickland et al., 1984a).

We complete this discussion with the third topic listed above. Most of the work reported in the following sections has already been documented elsewhere. The next section provides a synopsis of the major

document to be generated in this contract (the report just referenced above). The appendices contain papers either published or under review. Section 4 contains a revised internal report originally prepared for Huffman at AFGL. The subject deals with instrumentation and gives requirements for the detection of key optical features in the nighttime, daytime, and auroral ionospheres. This represents a beginning to an obviously critical part of the program, if the concept is to lead to an operational system. Section 5 discusses a small effort directed to analysing data from a daytime rocket experiment. The experiment provided the opportunity to analyze coincident optical and EDP data. Such analyses are critical to placing error bars on EDPs to be deduced from optical data.

Table 1. Breakdown of contract work by region of the ionosphere

Catagories:	NIGHT	DAY	AURORA
Code development	x		
First principles modeling		x	x
Empirical Modeling	x		
Literature Survey	x		
Gathering data	x	x	
Analysing Data	x	x	x
Detectability			
Backgrounds	x		
Instrumental characteristics	x	x	x
Statistics	x		
Reporting	x	x	x

3. The Proposed UV Ionospheric Monitoring System

Much of the work we performed under this contract was described in Strickland et al. (1984a). Rather than repeat that material here, we have chosen to provide a synopsis based on the executive summary of that report. The effort was directed toward developing a system concept for a satellite-borne optical sensor and the associated data analysis software that would be capable of providing electron density profiles over much of the globe and in near real time.

3.1 The System Concept

The system concept includes (a) developing and installing a UV sensor on the DMSP satellite and developing an associated automatic data processing (software) system, (b) using the optical data with DMSP electron density and temperature data to deduce the near real-time EDP near the satellite orbital plane, and (c) transmitting the EDP data for use with ground-based ionosonde data and GPS total electron content (TEC) data to specify the global EDP for system users. The ionosonde and TEC data would serve two purposes: to augment the EDP data base generated by the UV data, and to refine the UV-based EDP where coincident data exist.

3.2 The Ionospheric Subregions

We have considered the following ionospheric subregions: (a) the daytime low- to mid-latitude ionosphere from 90 to 1000 km, (b) the nighttime mid-latitude ionosphere from 250 to 1000 km, and (c) the auroral E layer from 90 to 200 km for undisturbed conditions. The spatial resolution considered for the daytime and nighttime EDP is at least one vertical profile for each square 500 km on a side and for the auroral E layer, at least one vertical profile for each 50 km on a side. Because of the high frequency of occurance of irregularities or of highly variable transport conditions, the polar caps, the cusp, the auroral F region, and the equatorial nighttime region were excluded from consideration.

3.3 Use of UV Measurements

(a) In the daytime low- to mid-latitude ionosphere there are no useful optical emission features which, when measured from the DMSP altitude (840 km), give a signal directly dependent upon the electron density profile. Therefore, we propose an indirect method in which we measure the emission feature at 1356 A and at least one of the Lyman-Birge-Hopfield (LBH) bands to deduce the O to N_2 density ratio and the absolute scale of the solar flux. This information and a neutral wind model are used to calculate the EDP from first principles using time dependent ion continuity equations. Basing the specified EDP on the deduced key parameters (O to N_2 density ratio and scaling factor for the solar flux) significantly improves the accuracy of the EDP over a result based on empirical values of these parameters.

(b) In the nighttime mid-latitude ionosphere there are at least two usable emission features which give a signal that is directly dependent on the EDP. The emission features are the atomic oxygen lines at 1356 A and 6300 A. These features are most sensitive to the electron content near and below the peak of the EDP. To extract the most accurate EDP from these observations, we are investigating two approaches: (i) a time dependent transport approach in which the neutral winds and possibly the electric fields are deduced from the optical emission measurements, and (ii) use of an empirical model in which the shape of the F layer is fixed and its location in altitude and its absolute value are determined by the emission features. This would produce F layer profiles from about 250 to 1000 km.

(c) For the E layer of the diffuse aurora we can use the emission feature at 1356 A and one or more of the LBH bands to determine the hardness and energy flux of the incident auroral electrons which produce the ionization. The EDP is then determined from 90 to about 200 km using this incident electron information in our electron transport/chemistry model.

3.4 Uncertainties

We have found that the proposed observables can provide a large fraction of the required 90-1000 km global coverage (see Table 2), as well as the bonus of sensing a broad area (rather than a single line) under the sub-orbital track. The feasibility of this approach rests upon our own recent advances in state-of-the-art capabilities simultaneously pressed into parallel areas: hardware development of UV sensors capable of measuring complete global day and nighttime emissions, and physical modeling of ionospheric processes strongly coupled to selected optical emissions. The hardware development has demonstrated success on both a shuttle flight and a recent satellite project; the software development has been successfully tested against field experimental data.

AVAILABLE OPTIONS

SUBREGIONS	UV	TOPSIDE SOUNDER	X-RAY
• Daytime low- to mid-latitude			
Bottomside	Yes	No	No
Topside	Yes	Yes	No
• Nighttime low- to mid-latitude			
Bottomside	Yes	No	No
Topside	Yes	Yes	No
• Auroral zone			
E Layer	Yes	No	Yes
D Layer	No	No	Yes

Table 2. Capabilities of Three Methods for Remote Sensing of the Ionosphere

Very few data exist for quantitative determination of error bars for

this EDP system concept due to scarcity of coincident optical and EDP measurements. For the present, the expected EDP improvement must be discussed in relative terms rather than in absolute terms. Nevertheless, meaningful statements can be made.

Errors in our ab-initio daytime model are comparable to those of the other state-of-the-art models for known conditions (order ± 30%). The factors of prime importance, as noted in Section 1.3, are the solar EUV flux, the O/N_2 density ratio, and the neutral wind. Errors in excess of a factor of 2 can be expected in the calculated EDP without direct knowledge of these factors. Optical observations will provide the needed knowledge for the first two factors and should lead to acceptable accuracy in the E and lower F regions. Near and above the peak of the EDP, transport effects are important. Further, overall errors should be significantly reduced with the aid of ionosonde and TEC data cited previously. Such data allow spot checking of the UV-deduced EDP through which adjustments can be made for such factors as optical sensor degradation.

Errors in deduced nighttime n_e profiles arise from variable transport and uncertainties in temperature and light ion composition. The major effects of variable transport are changes in the overall magnitude of the EDP and location of the EDP maximum. A less important effect is a change in the EDP shape. The proposed observables directly specify both the electron concentration near the peak and the height of the peak, thus eliminating most of the uncertainty caused by variable transport. The less important shape change remains a source of EDP error for this approach, being perhaps 20 to 30 percent at times of strong transport. Topside effects due to temperature and light ion composition are likely to be significant. The optimum approach to merging the information from optical emissions with information from in situ sensors remains to be determined.

In the auroral E layer, for arc-free conditions, determination of the EDP from 90 to 200 km should be achievable to within ± 40% by the method proposed in this report.

4. Instrument Requirements for a Global Ionospheric Monitoring System

4.1 Introduction

The system concept described in the preceding section involves the use of optical data, in situ plasma data, and a software data analysis system. We have made a considerable effort to determine the characteristics of the optical sensors that are necessary for determining the EDP to the described accuracy. The system is intended to monitor three regions:

(1) daytime low- to mid-latitude ionosphere from 90 to 1000 km
(2) nighttime mid-latitude ionosphere from 250 to 1000 km, and
(3) the auroral E layer from 90 to 200 km.

Monitoring is to be done under quiescent plasma conditions. The spatial resolution for the day and night EDP is to be at least one vertical profile for each square 500 km on a side and, for the auroral E layer, at least one profile for each square 50 km on a side.

The system is intended for use on DMSP satellites, which are placed in sun synchronous orbits, that is, orbits which always cross the equator at the same local time. There are two such orbits in use. One is approximately noon-midnight; the other is approximately dawn-dusk. The noon-midnight orbit is shown in Figure 1. It crosses the equator at local times of 10:30 am and 10:30 pm. The dawn-dusk orbit is also displaced from its nominal local time and actually crosses the equator before dawn and before dusk.

4.2 Optical Emissions

Table 3 lists some of the candidate optical features and nominal column emission rates for the three global regions of interest. The absence of a value indicates that the given feature is not useful for EDP monitoring in that region. The nighttime values are very small and have important implications for system design. However, these emissions are

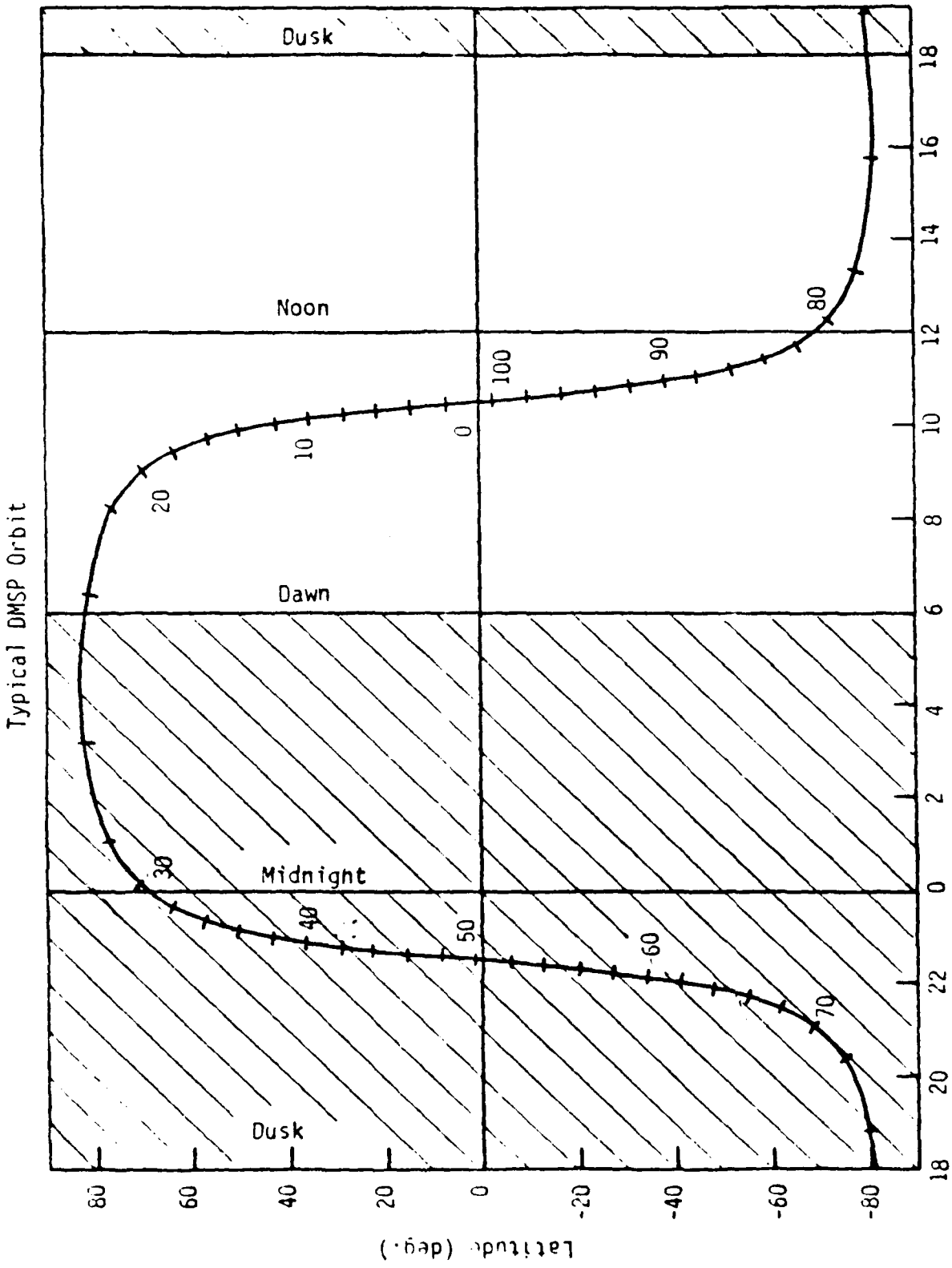

Figure 1. A typical DMSP noon-midnight orbit. Note that the orbit actually crosses the equator at 1030 and 2230 hr. The tick marks on the orbit track are two minutes

very attractive since they provide direct signatures of the EDP. Photometers will be needed to accurately measure them. Emissions in the day and during auroral activity are much brighter. A UV spectrometer will be capable of monitoring them on time scales of interest. The capability should be present to produce images (as was done on HILAT with the AIM instrument).

Monitoring the 6300 A emission at night presents special challenges beyond its inherent weakness. Part of the problem can be seen in Figure 2. The spectrum comes from Broadfoot and Kendall (1968) and shows the presence of other emissions. In particular, unwanted emission comes from OH rotational lines and from backscattered astronomical light. In addition, a nadir viewing instrument will register photons reflected from the ground or clouds as well as photons coming directly from the emitting layer. We propose the use of a tilting filter photometer or equivalent system to monitor both the signal and background.

Examples of partial FUV spectra for day and auroral conditions are shown in Figure 3. These were calculated for the conditions shown and provided intensities for additional features not shown in Table 3. We observe variability with changing conditions, which is the key to using the proposed features for EDP monitoring.

Feature	Day	Mid-latitude Night	Auroral E Layer
1356	100 - 3000	.1 - 4	100 - 1000
1304	1000 - 20,000	.2 - 10	1000 - 10,000
911	-	.05 - 2	-
1273	5 - 50	-	10 - 50
1325	10 - 100	-	20 - 100
1383	20 - 200	-	30 - 150
6300	-	2 - 100	-

Table 3. Nominal Ranges of Column Emission Rates in Rayleighs as observed from DMSP Satellite Altitude. (Lack of entry indicates feature is not to be used in given region.)

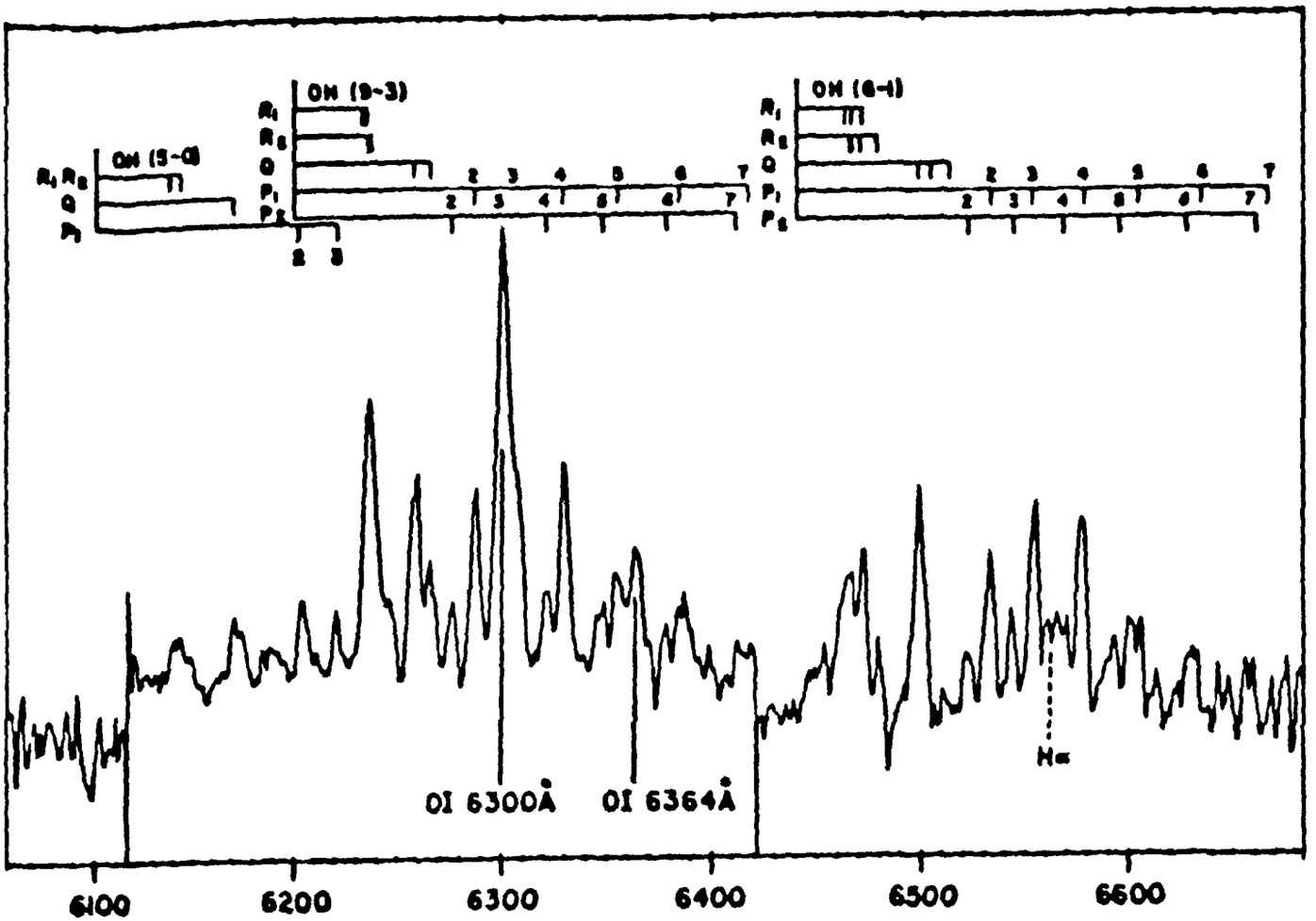

Figure 2. A ground-based airglow spectrum showing OI 6300 A, the OH lines, and the astronomical background (Broadfoot and Kendall, 1980).

Aurora

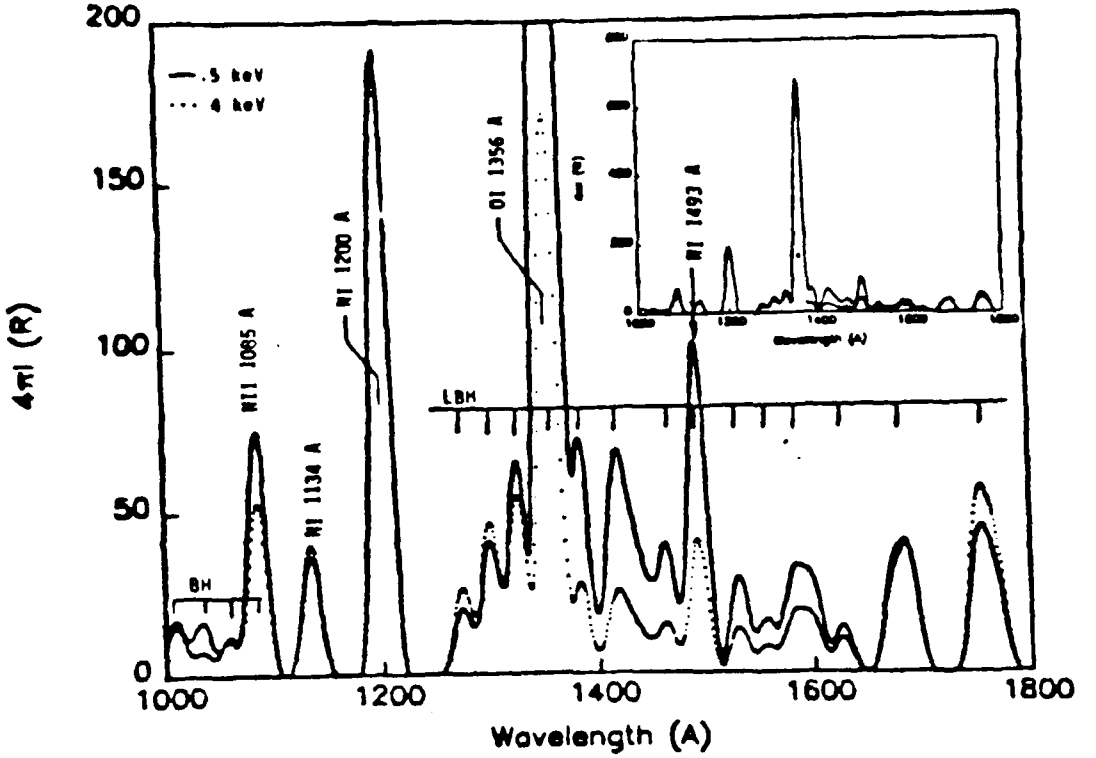

Day

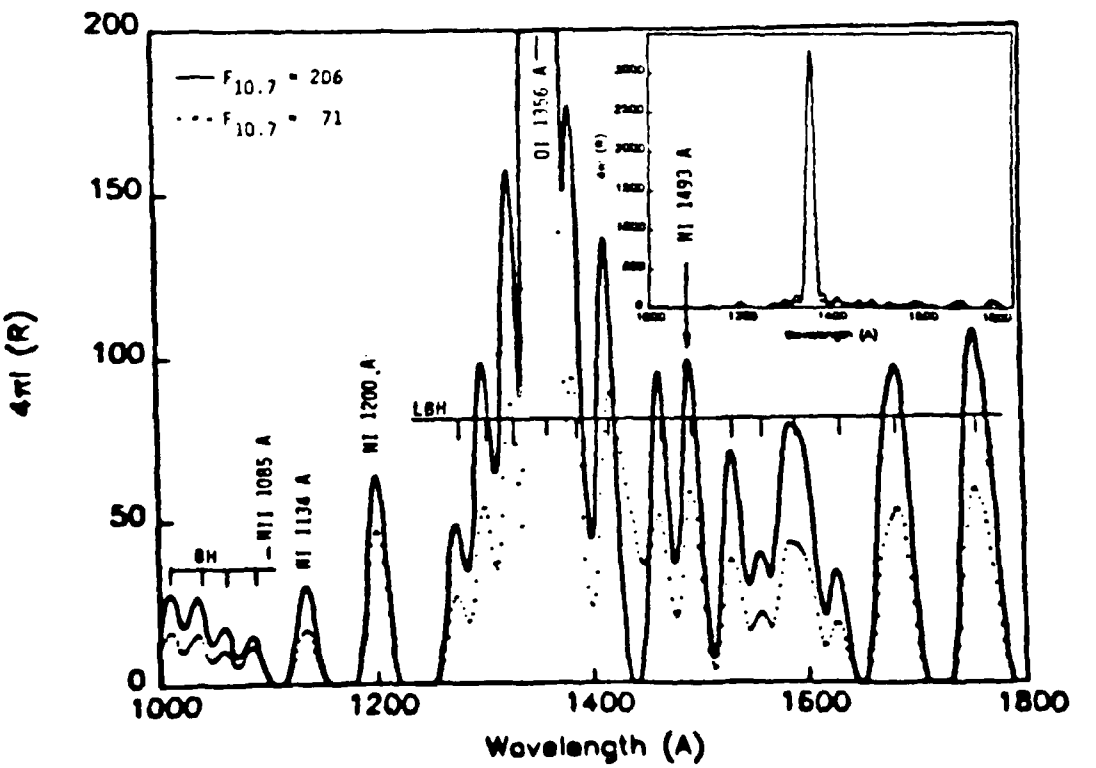

Figure 3. Calculated nadir viewing UV spectra for auroral and daytime conditions.

4.3 The Monitoring System

The ideal optical monitoring system would use the same instrument to monitor all three regions of interest. Unfortunately, the different characteristics of the dayglow, nightglow, and aurora cause difficulties in designing an instrument that can make acceptable measurements in all three environments. A high resolution instrument is reguired for measurements of the important UV spectral features in the dayglow and aurora. These features include OI 1356 A and N_2 LBH bands at 1383 A, 1672 A, and 1768 A. It would be highly desirable to monitor the 1356 A feature and one or more of the LBH bands simultaneously. This will be done by the AFGL UV imager on the Polar Bear Satellite. At night, instrument sensitivity is more important than resolution. The UV features of interest are OI 1356 A and OI 1304 A, which may be observed together by a wide band photometer. In addition, the OI 6300 A line must also be monitored, and that monitoring requires a separate photometer. Thus, the complete system should consist of an imaging UV spectrometer capable of observing two or more features simultaneously, a UV photometer, and a visible photometer.

To quantify the measurement requirements, we introduce R, the instrument response function (or sensitivity), which applies to any optical system. It is

$$R = (10^6/4\pi)\, A\Omega QT \qquad \text{counts Rayleigh}^{-1}\ \text{sec}^{-1}$$

where

- A is the area of entrance aperture, (cm^2)
- Ω is the viewing solid angle, (sr)
- Q is the quantum efficiency, and
- T is the transmission function

The scaling factor of $10^6/4\pi$ allows R to be expressed in terms of Rayleighs.

In the following discussion, we specify the minimum value of R that

an instrument must have to make the measurements with the required accuracy. We do not specify values for aperture, solid angle, or other parameters, because they are also constrained by engineering requirements that we have not addressed. We have found that in some cases the required instrument response is much greater than the response that can be readily obtained. For reference, we note that Huffman et al. (1980) describe a UV spectrometer with R = 55 counts R^{-1} s^{-1}. (This instrument was flown on the satellite S3-4. The UV photometer flown on the same satellite had R = 1200 counts R^{-1} s^{-1}.)

Let C be the total observed count rate, D the observed dark count rate, and S the counting rate due to the signal. Then

$$S = C - D \tag{1}$$

If the instrument counts for a time t, then the statistical uncertainties in these quantities are

$$s_C^2 = Ct \tag{2}$$

$$s_D^2 = Dt \tag{3}$$

$$s_S^2 = s_C^2 + s_D^2 = (C + D)t = (S + 2D)t \tag{4}$$

Away from the auroral zone, the dark count rate is constant, and S is simply $4\pi I$ R, where R is the previously defined instrument response, and $4\pi I$ is the apparent column emission rate of the signal.

In general, we wish to specify a maximum acceptable value for the relative uncertainty, $u_S = s_S/S$. This value may be expressed in terms of R and t:

$$u_S = \frac{\sqrt{4\pi IR + 2D}}{4\pi IR\ t} \tag{5}$$

Solving this expression for R, we obtain an expression for the instrument response that is necessary to obtain a specified statistical uncertainty

in a specified counting time:

$$R = \frac{1 + \sqrt{1 + 8u_S{}^2 Dt}}{2(4\pi I)u_S{}^2 t} \qquad (6)$$

This expression was used to drive the values given in Tables 4-6.

Table 4 gives required R values for various integration times, assuming the instrument is recording the minimum 1356 A column emission rates listed in Table 3. (0.1 Rayleighs at night and 100 R for the daytime and aurora). The R values are based on the accumulation of 25 counts of real signal in the absence of either dark counts or background emission. Thus, Table 4 applies to ideal conditions leading to a statistical uncertainty of 20 percent. An uncertainty greater than 20 percent leads to unacceptable uncertainty in the deduced electron density.

Integration Time (sec)	Nighttime (0.1 Rayleighs)	Day and Aurora (100 Rayleighs)
.1	2500	2.5
.2	1250	1.25
.5	500	.5
1.	250	.25
2.	125	.125
5	50	.05
10	25	.025

Table 4. Instrument Response, R (counts/R-sec), Required to Detect the Indicated Minimum Expected OI 1356 A Intensity With a Statistical Uncertainty of 20 Percent or Less. (No dark counts.)

Table 5 includes required R values similar to those listed in Table 3 but for more realistic conditions. In Table 5, we introduce a dark count rate of 6 count/s. We chose this value based on examples of the rate given by Huffman et al. (1980). Again, the given R values lead to 20 percent uncertainty.

Integration Time (sec)	Nighttime (0.1 Rayleighs)	Day and Aurora (100 Rayleighs)
.1	2600	2.61
.2	1360	1.4
.5	600	.60
1	340	.34
2	200	.20
5	110	.11
10	70	.069
20	45	.045
60	25	.025

Table 5. Similar to Table 2 Except for the Presence of a Dark Count Rate of 6 count/s.

The required R values for 100 Rayleighs of OI 1356 A do not strain instrument specifications, even for short integration times like 0.1s. At 0.1 Rayleighs, however, the necessary counts are not collected until integration times approaching one minute are applied. The DMSP satellite will cover a distance of ~ 450 km along its orbital path in one minute. A single data point over 450 Km distance will be unacceptable in situations where n_e is noticeably changing on shorter distance scales.

The R values in Table 5 demonstrate that existing UV spectrometers cannot reliably detect the minimum nighttime OI 1356 A intensity. Therefore, we propose the inclusion of a UV photometer similar to that flown on S3-4 (Hutfman, 1980). The photometer can be designed either to detect only OI 1356 A line, or to detect both OI 1356 A and OI 1304 A simultaneously. In the latter case, the minimum nighttime intensity of the combined features is about 0.3 R. The required instrument responses for both cases and for various integration times are shown in Table 6. The dark count rate is the same as for the S3-4 photometer. Since the S3-4 photometer had R = 1200 counts R^{-1} s^{-1}, it is clear that existing technology can provide accurate measurements with reasonable integration times. Using a filter wheel, the same photometer could also be used to

monitor one or more N2 LBH bands. These bands occasionally obscure OI 1356 A at night.

Integration Time (sec)	Nighttime			
	No Dark Counts		Dark Count Rate of 4 counts/sec	
	1356 alone	1356 & 1304	1356 alone	1356 & 1304
.05	5000	1700	5100	1700
.1	2500	830	2600	860
.2	1300	420	1300	440
.5	500	170	570	190
1	250	83	310	100
2	130	42	180	60
5	50	17	93	31
10	25	8.3	59	20

Table 6. Instrument Response Required to Detect OI 1356 A Alone and in Combination with OI 1304 A.

To monitor the nighttime 6300 A airglow, we propose to use a tilting filter photometer or its equivalent. This airglow measurement is complicated by the presence of two background sources. One background source is OH airglow emission, which can be comparable in intensity to OI 6300 A. The other source is reflected light from astronomical sources. At new moon, this source is almost negligible. At full moon, reflected moonlight can be as much as 100 times larger than the OI 6300 A line. Besides subtracting the background, we must also correct for that part of the OI 6300 A intensity that is reflected from the surface. Because of these complications, we must discuss the instrument design in more detail.

Because the astronomical background is broadband, it is most desirable to use a filter with the most narrow possible bandwidth. Filters for use at visible wavelengths can be made with bandwidths of 2.0

to 2.5 A. Unfortunately, this narrow bandwidth can be achieved only if the field of view is about 0.01 sr or less. To subtract the background, without introducing an unacceptable statistical uncertainty and with reasonable integration times, we may have to increase the field of view by about an order of magnitude. Thus, the filter bandwidth will be increased to 5 to 10 A. Introducting of optics in front of the filter to increase the effective collecting area has the same effect.

Although we performed an extensive quantitative analysis of the detectability of OI 6300 A in the nighttime ionosphere under this contract, we will not report it here because it has been superseded by a more recent analysis that we have performed under a contract with the Applied Physics Laboratory (APL) of Johns Jopkins University. The latter analysis is based on more complete and more accurate information concerning the OI 6300 A airglow, the sources of background, and optical instrument capabilities. This analysis confirms our previous conclusion that the measurement is feasible, but the quantitative results are sufficiently different to make presenting the findings of the old analysis uninform and misleading. The new analysis will appear in two reports being prepared by the authors. The first is being written in collaboration with J.R. Jasperse of AFGL and may be obtained from him when it is complete. The second is the final report for the APL contract mentioned above. It may be obtained from the authors when it is complete. (In both cases the most likely availability date is March 1985.)

The results of our most recent analysis may be summarized as follows: We assumed a hypothetical instrument with the following design parameters

$A = 19.6\ cm^2$ (50 mm filter, no optics)

$= 0.01$ sr (half cone angle = 3^0)

$Q = 9\%$

$T = 25\%$

$R = 312\ cts\ R^{-1}\ sec^{-1}$

For the actual local time of the "noon-midnight" DMSP orbit, OI 6300 A can be accurately measured by our hypothetical instrument under all moonlight conditions. This is true even in the mid-latitude trough. The longest integration time that will be required is about 4.3 seconds near 40^0 latitude at full moon. This includes the time required for observing the background intensities. In the mid-latitude trough, the longest integration time is about 3.7 seconds. Since the DMSP satellite moves at about 7.5 km/sec, this implies a spatial resolution of 28 km. As the instrument will probably have a field of about 0.01 sr, the actual spatial resolution will be about 85 km. This appears to be quite adequate to map the density gradients of the trough wall. There appears to be no need to augment the photometer with a telescope.

5. Preliminary Analysis of Data from a 1978 Dayglow Rocket Experiment

In this section, we describe an analysis of data from a dayglow rocket experiment conducted in 1978. The data include an EDP deduced from ground-based ionosonde data and UV intensities measured on board a sounding rocket. The data are coincident in that the respective instruments remotely sensed roughly the same region. This analysis came out of our effort to find experiments conducted in the dayglow, nightglow, and aurora that would provide both EDP's and UV intensities. The purpose for the search was to test our predictive capabilities, which is essential to the concept of deducing the EDP from satellite optical data. We must have confidence that our models can be used to predict the EDP, given that they are producing good optical results. We have found a 1978 dayglow rocket experiment that meets our criteria. Comparison between the data from this experiment and the results of our calculations has revealed that we cannot reproduce both the EDP and the optical data. We do not have the answer to this problem which is most pronounced at low altitudes ($\lesssim 120$ km). The same problem has been observed in similar comparisons with other ionosonde data. We plan to further investigate the problem jointly with J.R. Jasperse and D.W. Decker at AFGL.

The rocket experiment has been discussed by Gentieu et al. (1979), Meier et al. (1980), and Anderson et al. (1980). An analysis of the data appears in the Meier paper. The rocket was launched from White Sands Missile Range at 1300 MST on January 9, 1978. The solar zenith angle was 56^{o}. The prime experiments involved two spectrometers spanning the region from 530 to 1240 A. Data were recorded between 90 and 262 km for nadir, near zenith, and tangential viewing directions. The ionosonde data presented in this section were given to us by Paul Feldman (private communication, 1983) and, to our knowledge have not been published.

We have limited our calculations to the EDP and associated ion densities. Our optical intensities are the same as those generated by Meier et al. (1980) since we use the same photoelectron flux code and cross sections to produce the altitude profiles of volume emission. Intensities and their comparisons with data for selected emissions may be seen in Meier et al. (1980). A recent analysis by Meier and colleagues

(unpublished) has refined their earlier conclusions regarding atmospheric and solar conditions that were present during the 1978 rocket experiment. The following parameters reflect these conditions and have led to excellent agreement between predicted intensities and the spectrometer data (OI, NI, and N_2 features):

1) 960 K Jacchia (1977) model atmosphere

2) 1.1 times Torr et al. (1979) EUV solar spectrum indexed by $F_{10.7}$ = 71.

3) Donnelly and Pope (1973) soft x-ray solar spectrum

4) 0.6 times Stone and Zipf (1974) 1356 A electron impact cross section

We have used the information in parameters 1-3 to generate the calculated EDP shown in Figure 4. The calculations were done with our photoelectron code and with the auroral chemistry/optical emission code, which was modified for application to the daytime ionosphere. A calculated profile by Decker and Jasperse (personal communication) is included for comparison. They applied approximately the same conditions as listed above. Neither profile satisfactorily fits the ionosonde data, especially at the lower altitudes. The respective results came from first attempts to fit the data and, no doubt can be improved with certain parameter adjustments. Before adjusting parameters, however, we have decided to resolve the discrepancies between the two models producing these results. Resolving the discrepancies is being done by comparing detailed results such as the attenuated solar spectrum, primary ionization rates, and the photoelectron source spectrum at selected altitudes for the same model atmosphere and solar spectrum. A simplified spectrum is being used to facilitate the comparisons, especially those which include hand calculations. The comparison work will be reported at a later date. We can say, based on comparisons to date, that differences in the treatment of photoabsorption and photoionization cross sections are likely to be significant in producing the differences shown in Figure 4.

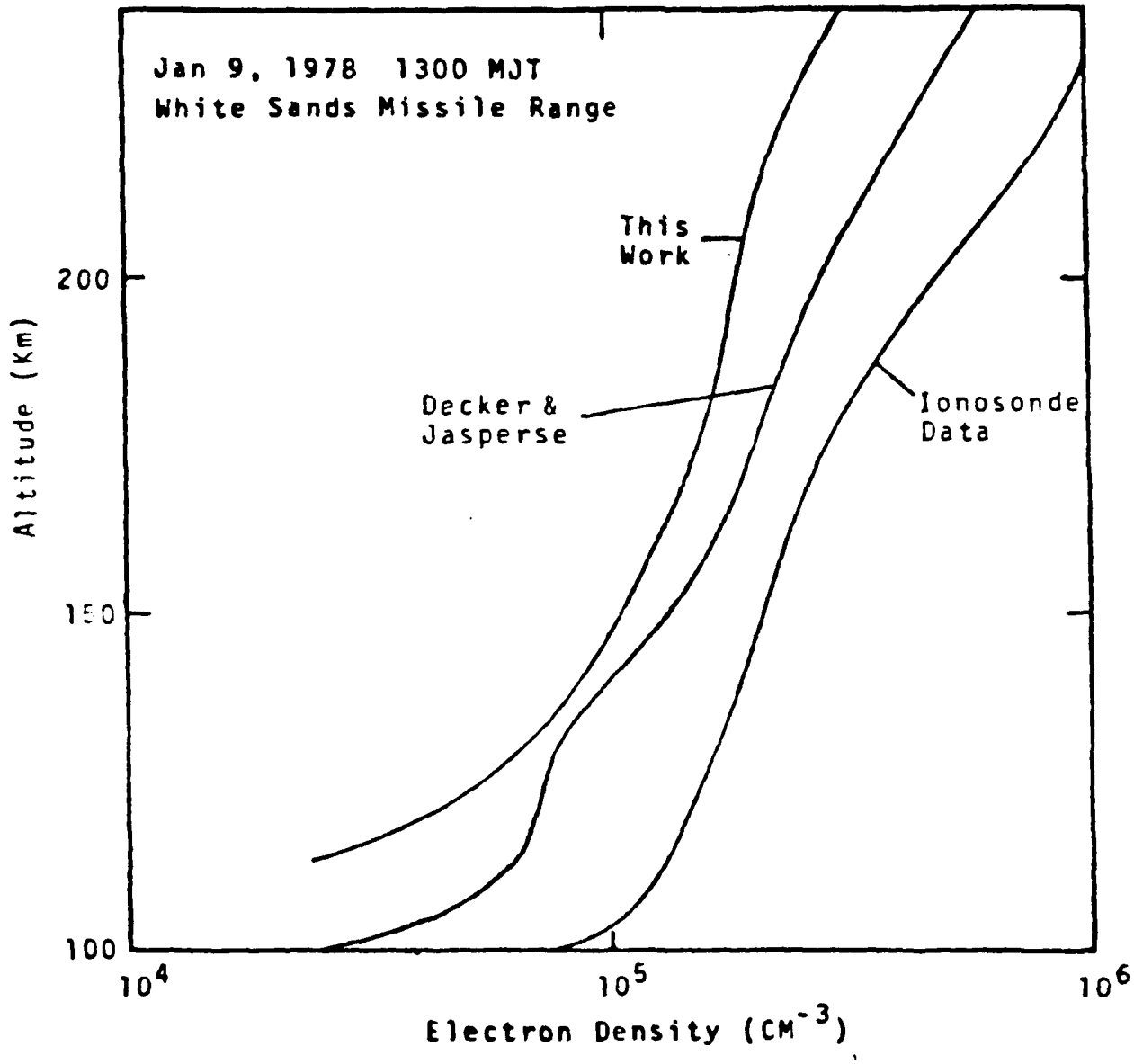

Figure 4. Calculated and measured EDP's above White Sands Missile Range on January 9, 1978 at 1300 MST. The calculated results are first attempts at fitting the data.

In summary, we observe that our predicted EDP lies below the EDP deduced from the ionosonde data by a factor of two and greater, depending on altitude. At the same time our predicted intensities for features such as OI 1356 A and LBH bands agree with the observations. To address this problem, we are making detailed comparisons with the results of Decker and Jasperse (personal communication)and will be examining in detail the key parameters leading from ionization rates to the corresponding EDP.

6. References

Anderson, D. E., Jr., R. R. Meier, P. D. Feldman, and E. P. Gentieu (1980). The UV dayglow 3, OI emissions at 989, 1027, 1152, 1304, and 1356, Geophys. Res. Lett., 7, 1057.

Broadfoot, A. L., and K. R. Kendall (1980). The airglow spectrum, 3100-10,000 A, J. Geophys. Res., 73, 426-428.

Daniell, R.E., Jr., D.J. Strickland, and J.R. Jasperse, Global Monitoring of the Ionosphere by Optical Techniques, IES Proceedings, 1984.

Daniell, R.E., Jr. and D.J. Strickland, Dependence of Auroral Middle UV Emissions on the Incident Electron Spectrum and Neutral Atmosphere, submitted to J. Geophys. Res., January, 1985.

Donnelly, R. F. and J. H. Pope (1973). The 1-3000A solar flux for a moderate level of solar activity for use in modeling the ionosphere and upper atmosphere, Tech. Rep. ERL 276-SEL 25, Natl. Oceanic and Atmos. Admin., Boulder, Co.

Gentieu, E. P., P. D. Feldman, and R. R. Meier (1979). Spectroscopy of the Extreme Ultraviolet Dayglow at 6.5 A Resolution: Atomic and Ionic Emissions Between 530 and 1240 A, Geophys. Res. Lett., 6, 325.

Huffman, R. E., F. J. Leblanc, J. C. Larrabee, and D. E. Paulsen. (1980). Satellite Vacuum Ultraviolet Airglow and Auroral Observations, J. Geophys. Res., 85, 2201.

Jacchia, L. G. (1977). Thermospheric Temperature, Density and Composition: New Models, Smithsonian Astrophysical Observatory Special Report 375.

Meier, R. R., D. J. Strickland, P. D. Feldman, and E. P. Gentieu (1980). The Ultraviolet Dayglow, 1. Far UV Emissions of N and N_2, J. Geophys. Res., 85, 2177.

Stone, E. J., and E. C. Zipf (1974). Electron impact excitation of the ^3S and ^5Sstates of atomic oxygen, J. Chem Phys., 60, 4237.

Strickland, D.J., J.R. Jasperse, and J.A. Whalen, Dependence of Auroral FUV Emissions on the Incident Electron Spectrum and Neutral Atmosphere, J. Geophys. Res., 88, 8051, 1983a.

Strickland, D.J., R.E. Daniell, Jr., S.. Chakrabarti, and R.C. McCoy, EUV Spectral Variations in Aurora - Comparison of Theory with Satellite Data, EOS, 64, 787, 1983b.

Strickland, D.J., R.E. Daniell, Jr., D. Decker, J.R. Jasperse, and H.C. Carlson, Determination of Ionospheric Electron Density Profiles from Satellite UV Emission Measurements, AFGL-TR-84-0140, May, 1984a. ADA150734

Strickland, D.J., R.E. Daniell, JR., and J.R. Jasperse, Using Satellite Observed UV Intensities to Deduce Electron Density Profiles, AIAA Journal, 22, 942, 1984b.

Torr, M. R., D. G. Torr, R. A. Ong, and H. E. Hinteregger (1979). Ionization frequencies for major thermospheric constituents as a function of solar cycle 21, Geophys. Res. Lett., 6, 771.

Whalen, J.A., General Characteristics of the Auroral Ionosphere, published in Physics of Space Plasmas, Ed. by T. S. Chang, B. Coppi, and J.R. Jasperse, SPI Conference Proceedings and Reprint Series, 4, Scientific Publishers, Cambridge, Ma., 1981.

Appendix A. Dependence of Auroral Middle UV Emissions on Incident Electron Spectrum and Neutral Atmosphere

by

R. E. Daniell, Jr.
and
D. J. Strickland

(submitted to the Journal of Geophysical Research, November 1984)

DEPENDENCE OF AURORAL MIDDLE UV EMISSIONS ON THE INCIDENT ELECTRON SPECTRUM AND NEUTRAL ATMOSPHERE

by:

R. E. Daniell, Jr.

BEERS ASSOCIATES, INC.
Post Office Box 2549
Reston, Virginia 22090

and

D. J. Strickland

COMPUTATIONAL PHYSICS, INC.
Post Office Box 360
Annandale, Virginia 22003

Submitted to:

JOURNAL OF GEOPHYSICAL RESEARCH

January 1985

Dependence of Auroral Middle UV Emissions on the Incident Electron Spectrum and Neutral Atmosphere

Abstract

In this paper we examine the relationship between two important middle UV auroral emissions, the electron energy spectrum, and the neutral atmosphere. Using both Maxwellian and Gaussian forms for the incident energy spectra, we show that the N_2 Vegard-Kaplan band system is sensitive to both the atomic oxygen density and the characteristic energy of the incident spectrum. This is due to quenching of the $A^3\Sigma_u^+$ state by atomic oxygen. (Since there remains some uncertainty about the magnitude of the quenching, we have used both large and small values in our calculations.) We also show that the second positive system of N_2 is much less sensitive to incident energy and atomic oxygen density. In principle, observations of these two emissions could be used to characterize the incident electron spectrum if the atomic oxygen density were accurately known from models or observations.

1. Introduction

In this paper, we present results showing emission properties for selected features within the N_2 Vegard-Kaplan (VK) and second positive (2P) systems. We wish to know how such features vary in relation to one another, and to other features as well, from one aurora to another. The variation results from changes in the incident electron spectrum and composition. Our interest here is in the middle ultraviolet (MUV) and for this region, the above mentioned systems provide the most prominent features, with the exception of 2972 A, which comes from $O(^1S)$. This feature will not be discussed here.

Relative variations among emission features offer the potential to deduce characteristics of the energy source and neutral composition from observations of their intensities. This provided the motivation for the work reported by Strickland et al. [1983] (hereafter, SJW) on prominent far UV (FUV) features. The work being reported here represents an extension of that work into the MUV region. There has been interest over the years in auroral emission variability, mainly as observed from the ground. Vallance Jones (e.g. Vallance Jones, 1975) and Rees (e.g. Rees and Luckey, 1974) have pioneered much of the work on this subject (a brief review is given by SJW). Here, we have in mind observations from satellites and the determination of their usefulness for mapping electron precipitation characteristics which in turn provides information on electron density profiles with the aid of models.

2. Atmospheric, Molecular, and Chemical Parameters

We have used the same model atmosphere as was used by SJW: the model of Jacchia [1977]. SJW also discussed the variability of neutral densities and compared the Jacchia model with observations. Following SJW, we have examined the effects of reducing the O density by as much as a factor of three.

The features we have investigated are the Vegard-Kaplan (VK) and the second positive (2P) band systems of N_2. A simplified energy level diagram for the triplet states of N_2 is given in Figure 1. In calculating Vegard-Kaplan intensities, we have made extensive use of the analysis of Cartwright [1978]. He found that the low-lying vibrational levels of the A state were populated largely by cascading from the B, B', C, and W states. Because cascading takes place on time scales that are short compared to the lifetime of the A state (about 2 seconds), the production of any of these states is tantamount to production of the A state. The only exception is the C state which predissociates approximately half of the time [Porter et al., 1976]. Therefore, we have calculated the total production of all levels of the A state by using an effective electron impact cross section σ_T:

$$\sigma_T = \sigma_A + \sigma_B + 0.5\sigma_C + \sigma_W \qquad (1)$$

which is shown in Figure 2. The individual cross sections were taken from Cartwright et al. [1977]. We apportioned the production among the A state vibrational levels according to the population rates given by Cartwright [1978].

In particular, we assigned 22 percent of the production to the v'=0 level and 16 percent to the v'=1 level. For transition probabilities, we have adopted the values given by Shemansky [1969].

The A state is affected by chemistry only through quenching. We have included quenching by N_2, O_2, N, O, and NO. Unfortunately, the quenching rate coefficient for the most important species, O, is also the most uncertain. (See Torr and Torr [1982] for review.) Sharp [1971] and Torr and Sharp [1979] deduced quenching rates of 9×10^{-11} cm^3 s^{-1} for the v'=0 level and 2×10^{-10} cm^3 s^{-1} for the v'=1 level (hereafter called the Sharp values). These determinations were based on rocket data. Ground-based auroral observations by Rees et al. [1976] and Vallance Jones and Gattinger [1976] yielded values about one-third as large. Laboratory measurements by Piper et al. [1981] agreed with the lower values: 2.8×10^{-11} cm^3 s^{-1} for v'=0 and 3.4×10^{-11} cm^{-3} s^{-1} for v'=1 (hereafter called the Piper values). Recently, McDade and Llewellyn [1984] have reanalyzed several sets of auroral emission data using the Piper values. Since they did not have measurements of the atomic oxygen density, they had to use a model. They obtained good agreement between theory and observation using the CIRA 72 model atmosphere, which provides support for the Piper values. However, the fact that their O density came from a model, rather than from observations, prevents the question from being conclusively settled. Consequently, the calculations presented in the next section were performed using both sets of values.

The N_2 2P system (arising from C to B transitions) is easier to deal with. Cascading from the D and E states is negligible, so the production rate consists only of direct excitation by electron impact. The

transition to the B state is allowed, so quenching is unimportant. The fraction of the total volume emission rate which appears in a given band is obtained from the product $q(v',0)\ A(v',v'')\ \tau(v')$ where $q(v',0)$ is the Frank-Condon factor for production of the v' level of the C state from the 0 vibrational level of the ground state, $A(v',v'')$ is the transition probability for the v'-v" transition, and $\tau(v')$ is the lifetime of the v' level. (We assume that in the ground state, only the lowest vibrational level is appreciably populated.) For the (0,0) band, this product has the value 0.27 [Vallance Jones, 1974]. The predissociation mentioned above affects only the higher vibrational levels of the C state, and is not important for the (0,0) band for which the calculations of the next section were done. We have used the previously-cited cross section [Cartwright, 1977] to calculate the C state production rate.

3. Calculated Volume Production Rates and Intensities

As in SJW, we have performed calculations for both Maxwellian and Gaussian incident electron energy spectra and for a range of characteristic energies typical of auroral conditions.

The Maxwellian spectrum may be represented by

$$F_M(E) = \frac{Q_M}{2\pi E_M^3} E \exp(-E/E_M) \tag{2}$$

where $F_M(E)$ is the electron flux at energy E, Q_M is the total energy flux, and E_M is the characteristic energy. We assume that the flux is isotropic over the downward hemisphere.

The Gaussian spectrum may be represented by

$$F_G(E) = \frac{Q_G}{\sqrt{\pi^3} W E_G} \exp\left[-\left(\frac{E-E_G}{W}\right)^2\right] \tag{3}$$

where F_G, and Q_G, and E_G are analogous to F_M, Q_M, and E_M. W is the width of the spectrum. (To be exact, the full width at half maximum is $2\sqrt{\ln 2}\, W$.)

Note that the mean energy of a Maxwellian spectrum is twice the characteristic energy: $\langle E \rangle_M = 2\, E_M$. In contrast, the mean energy of a Gaussian spectrum is equal to the characteristic energy: $\langle E \rangle_G = E_G$. This should be kept in mind when comparing calculations based on the two

different spectral forms. In all calculations presented here, we have chosen Q_M and Q_G to be 1 erg cm^{-2} s^{-1}. Since volume emission rates are directly proportional to Q, it is easy to scale the results to other values of the energy flux.

The altitude dependence of the production and loss terms for the lowest vibrational level of $N_2(A)$ are shown in Figures 3 and 4. The Piper values for quenching by atomic oxygen were used in Figure 3 and the Sharp values were used in Figure 4. The main effect of the higher Sharp values is to reduce the peak emission rate by a factor of two. A less significant effect is the lifting of the altitude of peak emission by about 5 kilometers. Altitude profiles of the volume emission rate of the (0,6) Vegard-Kaplan band at 2762 Å for various values of the characteristic electron energy are given in Figures 5 and 6. Note that even though the peak production rate increases with increasing electron energy (see Figure 3 and 4), quenching causes the peak volume emission rate to decrease.

Because quenching is not important for the C state, the volume emission rate for any band of the 2nd positive system is proportional to the production rate. In particular, the volume emission rate of the (0,0) band, which is not affected by predissociation, is equal to the production rate. The altitude dependence of the (0,0) band volume emission is shown is Figure 7. Note that in contrast to the Vegard-Kaplan system, higher energy fluxes produce greater peak volume emission.

4. Calculated Column Emission Rates

We have integrated the volume emission rates shown in Figures 5-7 to produce column emission rates as functions of electron energy. The results for the Vegard-Kaplan system are shown in Figures 8 and 9. We show two of the brightest bands of the system, as well as the sums of the v'=0 and v'=1 progressions. Except at the lowest energies, the intensity of the Vegard-Kaplan system decreases rapidly with increasing electron energy. This is the effect of quenching. Since the quenching rate is proportional to the atomic oxygen concentration, a reduction in the quenching coefficient by any factor is equivalent to an increase in atomic oxygen by the same factor. Thus, these two figures can also be taken as illustrations of the sensitivity of the emission to variations in oxygen density. That is, Figure 9 can be taken as the intensities that would be obtained if the Piper values were used, but with the oxygen density increased by a factor of three. (This neglects the second order effects due to the additional absorption of energy by the atomic oxygen, as it is increased relative to that of N_2.)

The energy dependence of the column emission rates for the (0,0) band of the 2nd positive system is shown in Figure 10. Although this intensity is a monotonically increasing function of energy, the rate of increase is not very rapid, especially at higher energies. At sufficiently low electron energies, most of the energy is deposited at high altitudes where atomic oxygen dominates. As the energy increases, a greater fraction is deposited in nitrogen, so the column emission also increases. However, when the electron energy is high enough, the energy is deposited at altitudes where atomic oxygen is not important,

so the column emission depends mainly on the total energy flux, and not on the characteristic energy. Although the peak volume emission rate does increase with characteristic energy, the emitting layer becomes thinner.

5. Discussion

The two band systems discussed in this paper could not be used to deduce the incident electron spectrum from optical observations without additional information. If the atomic oxygen density were known from other observations or from models, then these two emissions could, in principle, be used to calculate the energy content and mean (or characteristic) energy of the electron spectrum. This is because the two emissions have different dependences on characteristic electron energy, and are both proportional to the total energy flux. The main problem in making use of these emissions is their relatively low intensities. However, there are some other complications. One of these is the finite width of the bands. The rotational lines making up a band are spread over several Angstroms. The amount of spread depends on the rotational temperature of the emitting species. For example, if the effective rotational temperature of N_2 in the A state is 800 K, the VK (0,6) band is spread over approximately 60 Å. (We have not attempted to model rotational distributions for actual auroral conditions). Rotational spreading also causes the VK (0,9) band to overlap the 2P (0,0) band. Conway and Christensen [1984] modeled this contamination of photometer observations in the dayglow and concluded that 2P (0,0) band observations should be done spectrometrically rather than photometrically. This conclusion is almost certainly valid for auroral conditions as well.

There is a second complication for the (0,0) band of the 2nd positive system: Rayleigh scattering from the atmosphere below the emitting layer. This is not a problem at wavelengths shorter than 3000 A because of pure absorption by O_2. At the wavelength of the (0,0) band (3371 A),

there is very little absorption, but there is sufficient multiple scattering that most of the light emitted in the downward direction is scattered upward. Thus the apparent column emission rate inferred from satellite observations will be too large unless this effect is taken into account. (These statements are based on multiple scattering calculations of Anderson quoted in Strickland and Daniell [1982].)

Acknowledgements. We are grateful to R. Conway of the Naval Research Laboratory for several useful discussions concerning the Vegard-Kaplan system. This work was partially supported by the Air Force Geophysical Research Laboratory through contract F19628-83-C-0078 and the Applied Physics Laboratory through contract 602116-S.

References

Cartwright, D. C., Vibrational populations of the excited states of N_2 under auroral conditions, J. Geophys. Res., 83, 517-531, 1978.

Cartwright, D. C., S. Trajman, A. Chutjian, and W. Williams, Electron impact excitation of the electronic states of N_2, II, Integral cross sections at incident energies from 10 to 50 ev, Phys. Rev., Sect. A, 16, 1041-1051, 1977.

Conway, R. R., and A. B. Christensen, The ultraviolet dayglow at solar maximum. II. Photometer observations of N_2 second positive (0,0) band emission, submitted to J. Geophys. Res., 1984.

Jacchia, L. G., Thermospheric temperature, density, and composition: New models, Spec. Rep. 375, Smithsonian Astrophys. Observ., Cambridge, Mass., 1977.

Piper, L. G., G. E. Caledonia, and J. P. Kennealy, Rate constants for deactivation of $N_2(A^3\Sigma_u^+, v'=0,1)$ by O, J. Chem. Phys., 75, 2847-2852, 1981.

Porter, H. S., C. H. Jackman, and A. E. S. Green, Efficiencies for production of atomic nitrogen and oxygen by relativistic proton impact in air, J. Chem Phys., 65, 154-167, 1976.

Rees, M. H., G. G. Sivjee, and K. A. Dicke, Studies of molecular nitrogen band from airborne auroral spectroscopy, J. Geophys. Res., 81, 6046-6058, 1976.

Sharp, W. E., Rocket-borne spectroscopic measurements in the ultraviolet aurora: Nitrogen Vegard-Kaplan bands, J. Geophys. Res., 76, 987-1005, 1971.

Sharp, W. E. and D. G. Torr, Determination of the auroral O(^{1}S) production sources from coordinated rocket and satellite measurements, J. Geophys. Res., 84, 5345-5348, 1979.

Shemansky, D. E., N_2 Vegard-Kaplan System in Absorption, J. Chem. Phys., 51, 689-700, 1969.

Strickland, D. J., and R. E. Daniell, UV emissions and the electron density in the Auroral and low to mid-latitude daytime ionospheres, AFGL-TR-82-0373, Air Force Geophysics Laboratory, Hanscom AFB, Massachusetts, 1982. *ADA126318*

Strickland, D. J., J. R. Jasperse, and J. A. Whalen, Dependence of auroral FUV emissions on the incident electron spectrum and neutral atmosphere, J. Geophys. Res., 88, 8051-8062, 1983.

Torr, D. G., and W. E. Sharp, The concentration of atomic oxygen in the auroral lower thermosphere, Geophys. Res. Lett., 6, 860-862, 1979.

Torr, M. R., and D. G. Torr, The role of metastable species in the thermosphere, Rev. Geophys. Space Res., 20, 91-144, 1982.

Vallance Jones, A., and R. L. Gattinger, Quenching of the N_2 Vegard-Kaplan system in aurora, J. Geophys. Res., 81, 497-500, 1976.

R. E. Daniell, Beers Associates, Inc. P.O. Box 2549, Reston, VA 22090.

D. J. Strickland, Computational Physics, Inc., P.O. Box 360, Annandale, VA 22003.

Figure Captions

Figure 1. A simplified energy level diagram for the triplet states and band systems of molecular nitrogen. The two band systems discussed in this paper are the Vegard-Kaplan and 2nd positive sytems.

Figure 2. The total cross section for the production of the A $^3\Sigma_u^+$ state of N_2 by electron impact. This cross section takes into account cascading from higher lying states. (See text for complete explanation.)

Figure 3. Altitude profiles of the production and loss rates for the $v' = 0$ vibrational state of the A state of N_2 for (a) Maxwellian and (b) Gaussian incident electron spectra. The quenching rate was calculated using the Piper et al. [1981] values for the quenching coefficients.

Figure 4. Altitude profiles of the production and loss rates for the $v' = 0$ vibrational state of the A state of N_2 for (a) Maxwellian and (b) Gaussian incident electron spectra. The quenching rate was calculated using the Sharp [1971] and Torr and Sharp [1979] values for the quenching coefficients.

Figure 5. Altitude profiles of the volume emission rate of the (0,6) Vegard-Kaplan system for (a) Maxwellian and (b) Gaussian incident electron spectra. Profiles are shown for several characteristic energies. The Piper quenching coefficients were used.

Figure 6. Altitude profiles of the volume emission rate of the (0,6) Vegard-Kaplan system for (a) Maxwellian and (b) Gaussian incident electron spectra. Profiles are shown for several characteristic energies. The Sharp quenching coefficients were used.

Figure 7. Altitude profiles of the volume emission rate of the (0,0) band of the 2nd positive system for (a) Maxwellian and (b) Gaussian incident electron spectra. Profiles for several characteristic electron energies are shown.

Figure 8. The dependence of the column emission rate of the (0,6) Vegard-Kaplan band on the incident electron energy for (a) Maxwellian and (b) Gaussian electron spectra. The Piper quenching coefficients were used.

Figure 9. The dependence of the column emission rate of the (0,6) Vegard-Kaplan band on the incident electron energy for (a) Maxwellian and (b) Gaussian electron spectra. The Sharp quenching coefficients were used.

Figure 10. The dependence of the column emission rate of the (0,0) 2nd positive band on the incident electron energy for (a) Gaussian and (b) Maxwellian electron spectra.

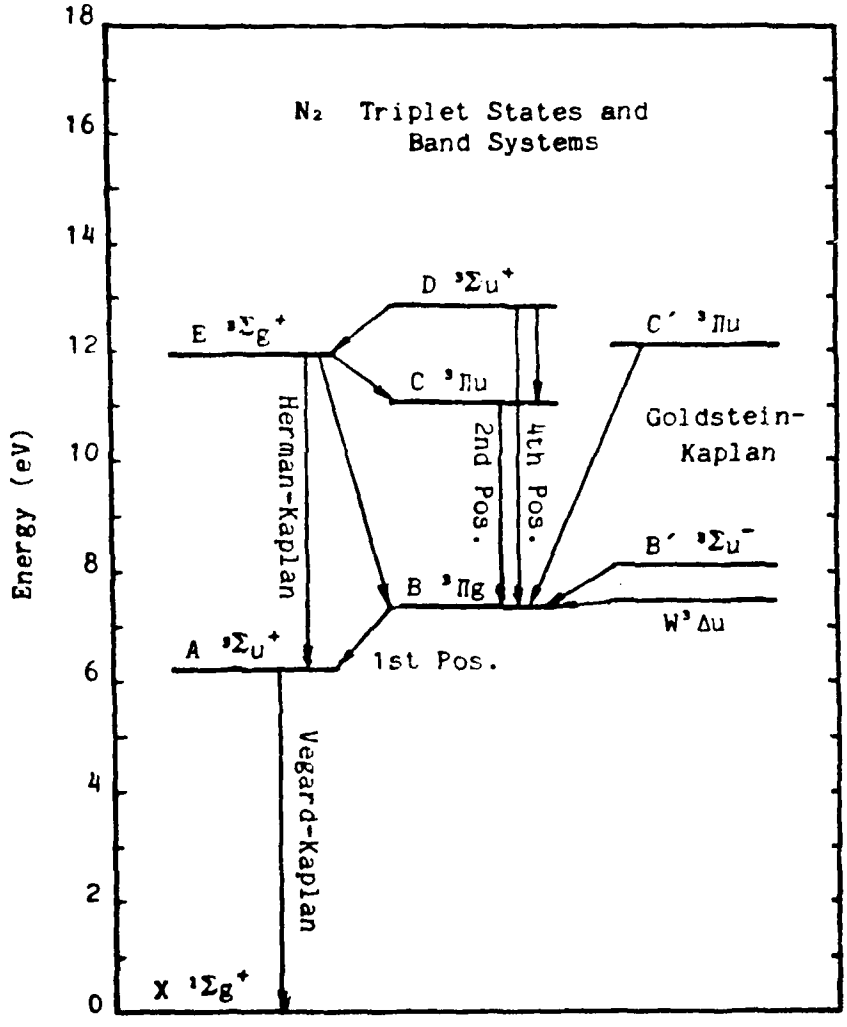
N₂ Triplet States and
Band Systems
Energy (eV)
18
16
14
12
10
8
6
4
2
0
D ³Σu⁺
E ³Σg⁺
C ³Πu
C´ ³Πu
Goldstein-
Kaplan
Herman-Kaplan
2nd Pos.
4th Pos.
B´ ³Σu⁻
B ³Πg
W³Δu
A ³Σu⁺
1st Pos.
Vegard-Kaplan
X ¹Σg⁺

figure 1

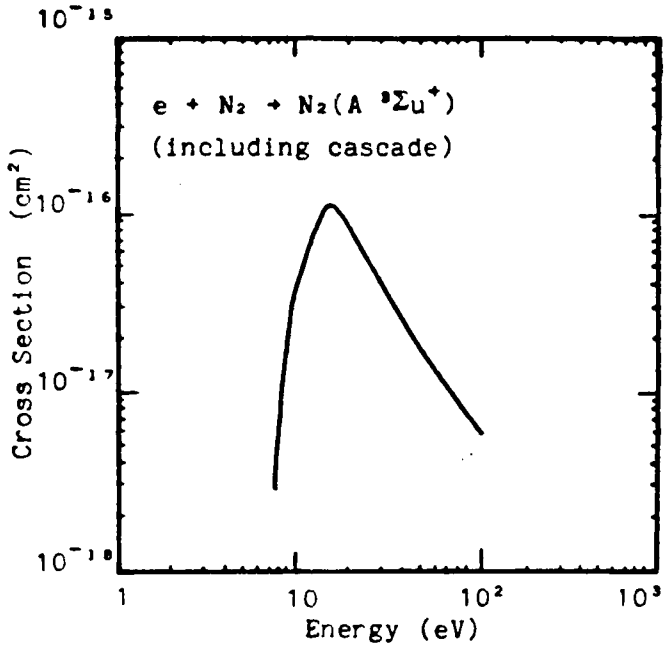
10^{-15}
10^{-16}
10^{-17}
10^{-18}
Cross Section (cm^2)
$e + N_2 \rightarrow N_2(A\ ^3\Sigma_u^+)$
(including cascade)
1
10
10^2
10^3
Energy (eV)

figure 2

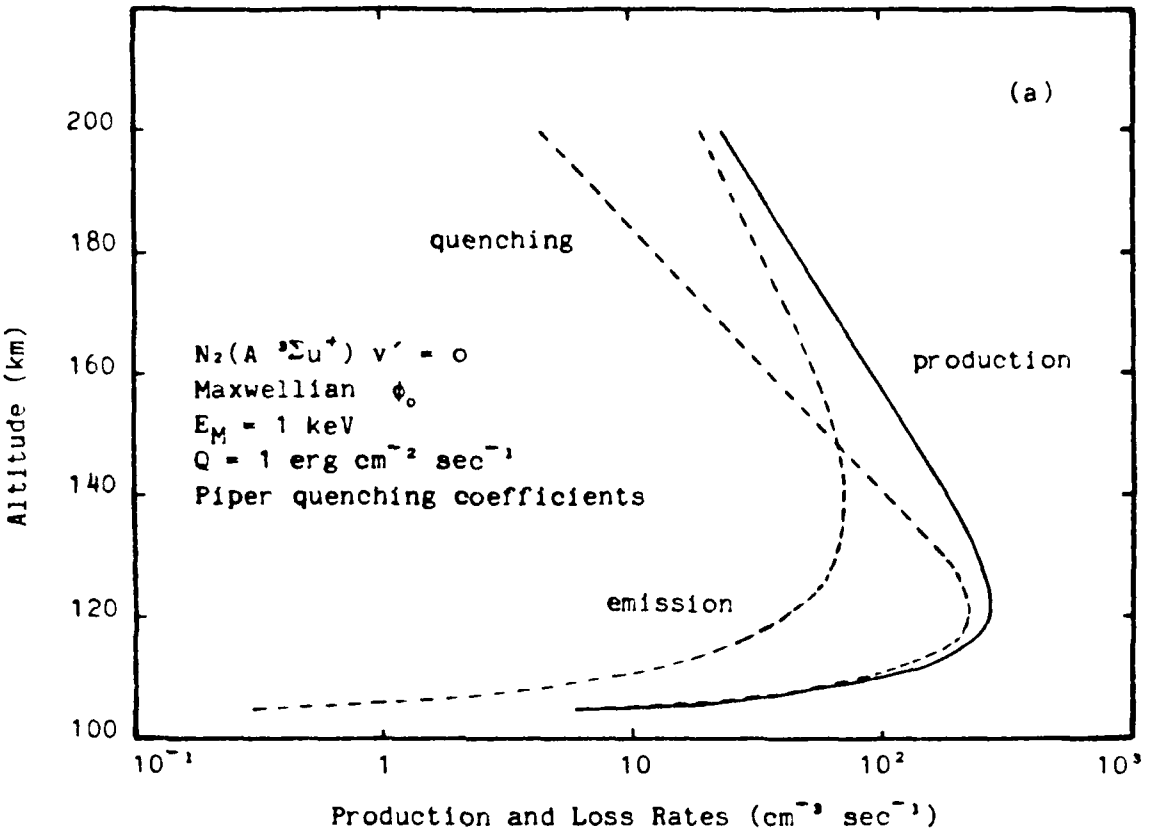

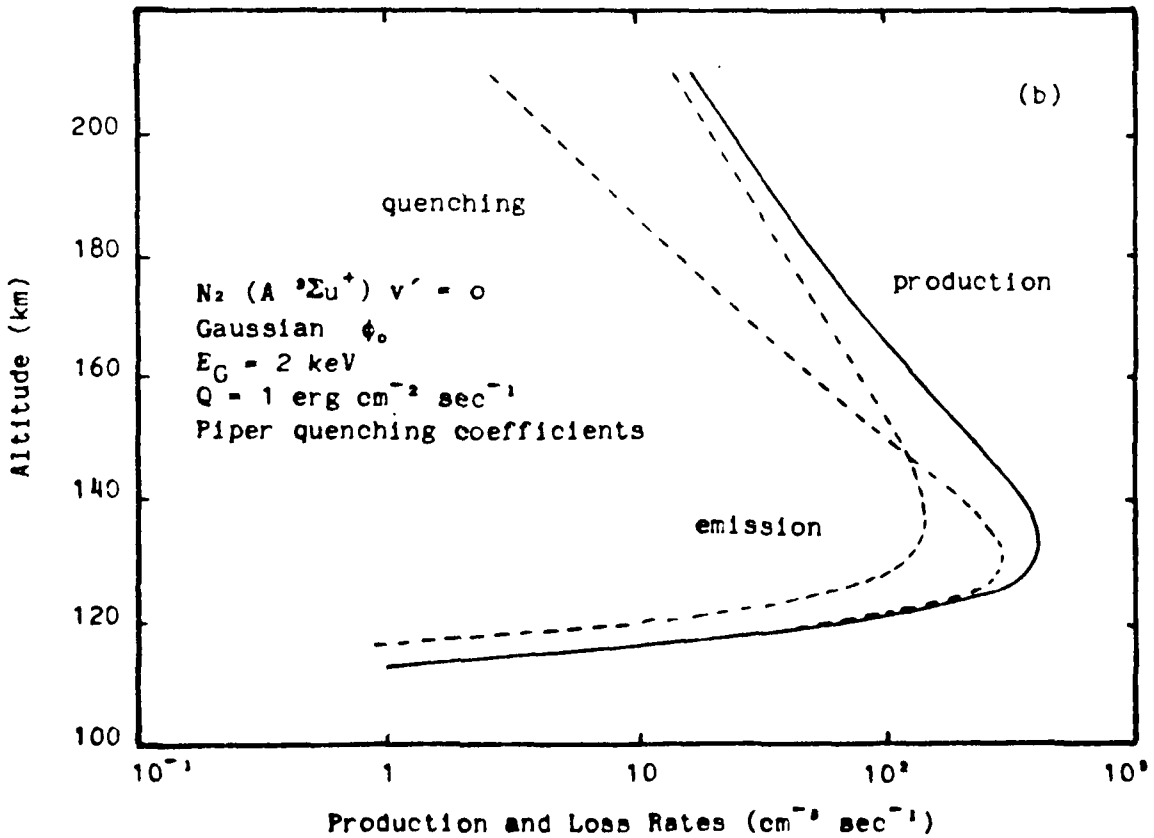

figures 3a and 3b

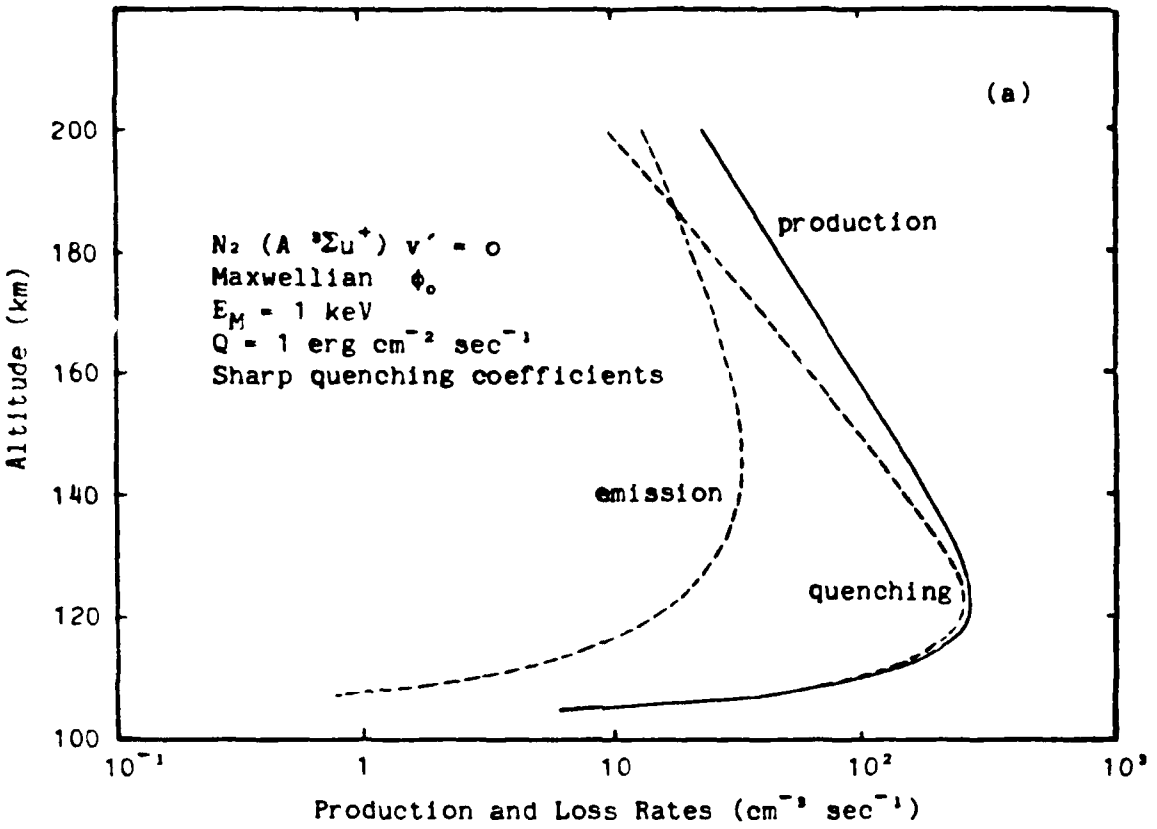

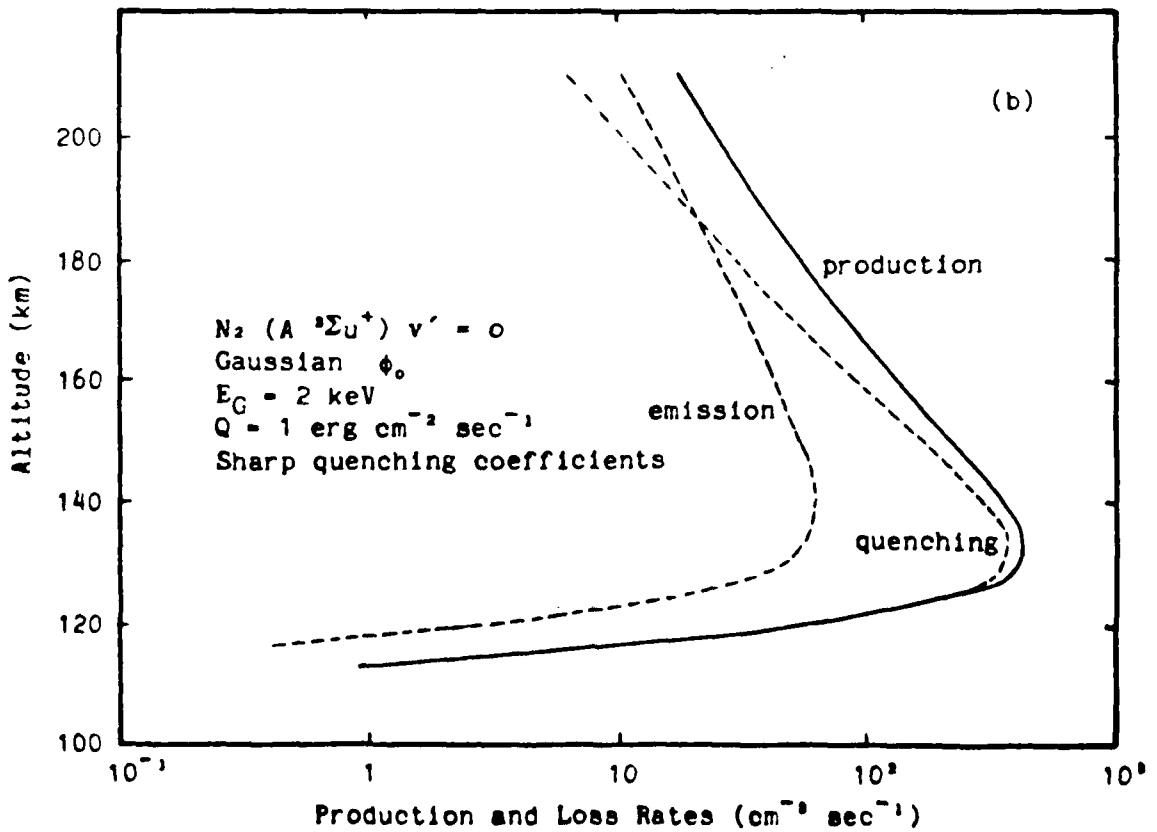

figures 4a and 4b

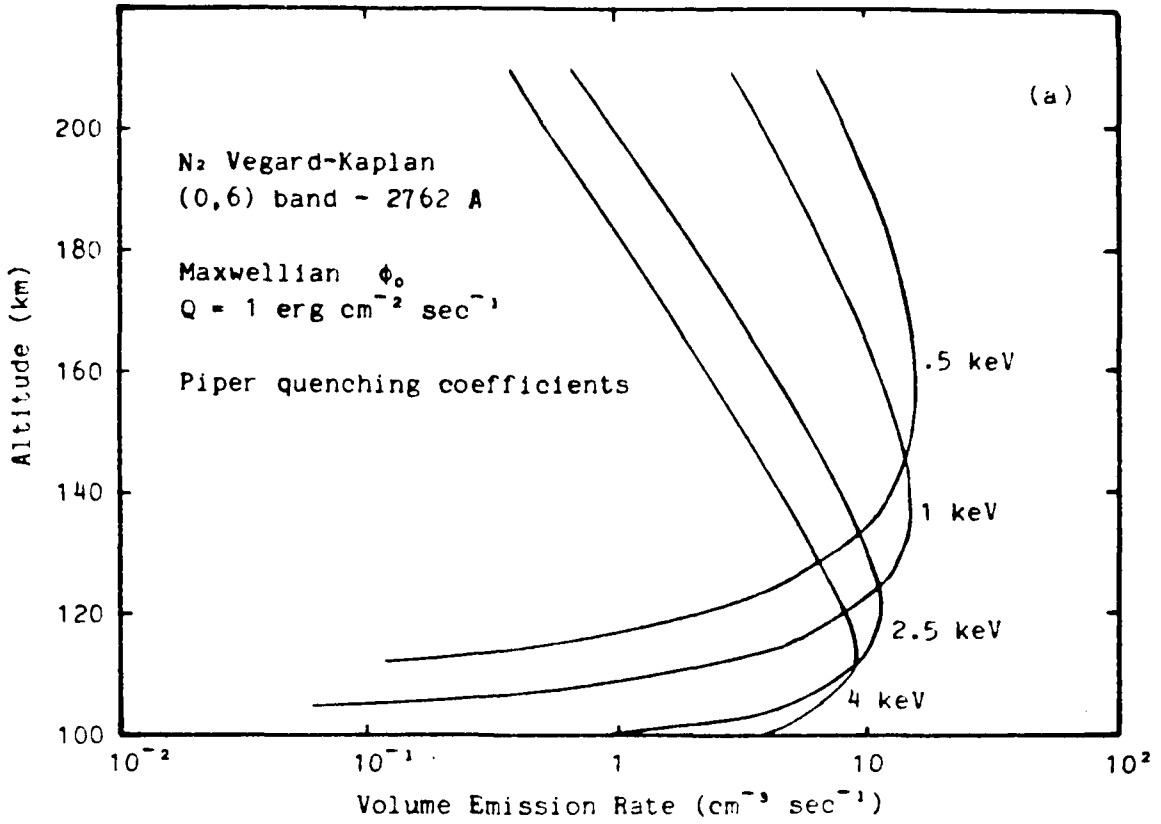

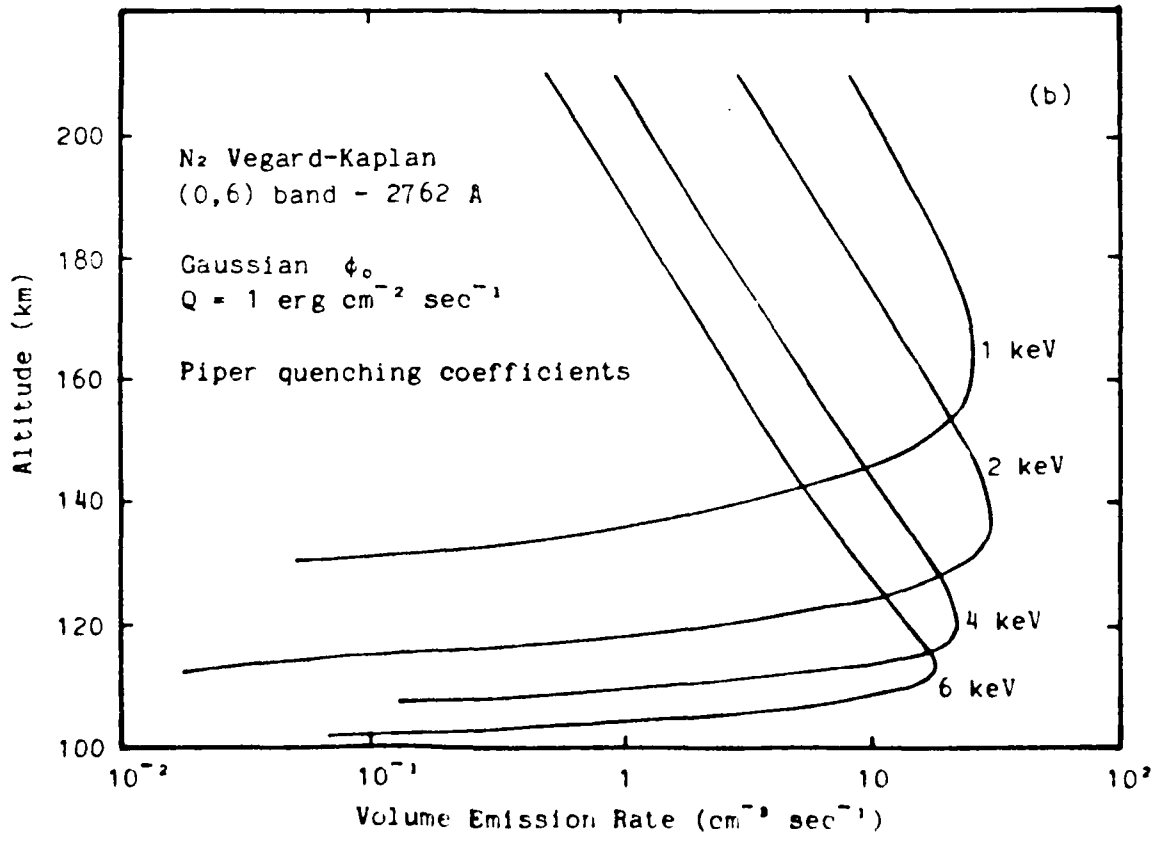

figures 5a and 5b

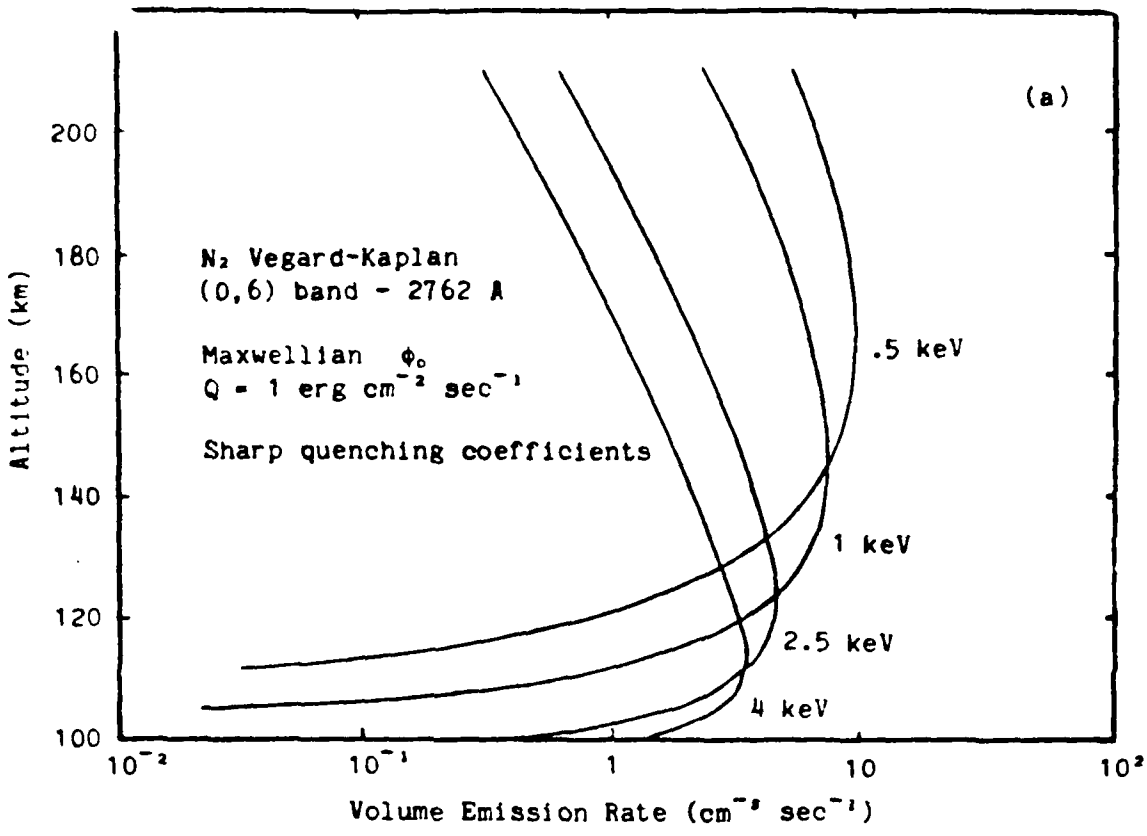

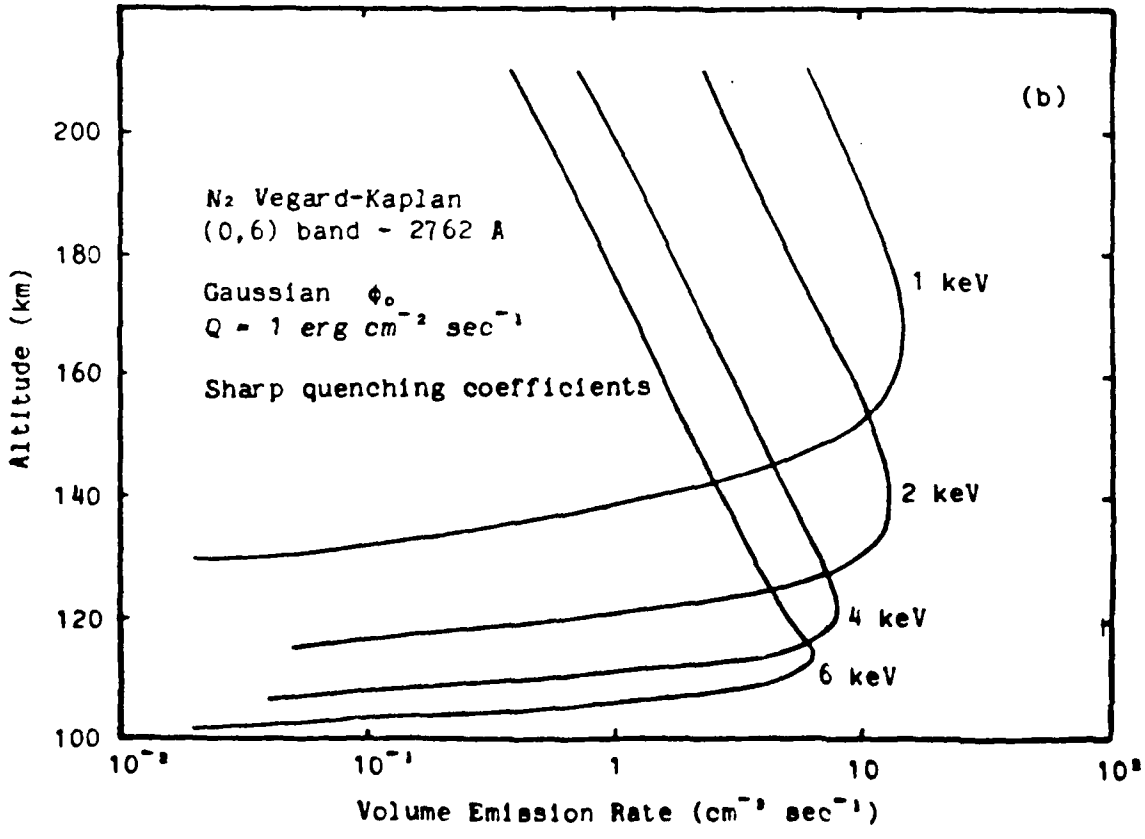

figures 6a and 6b

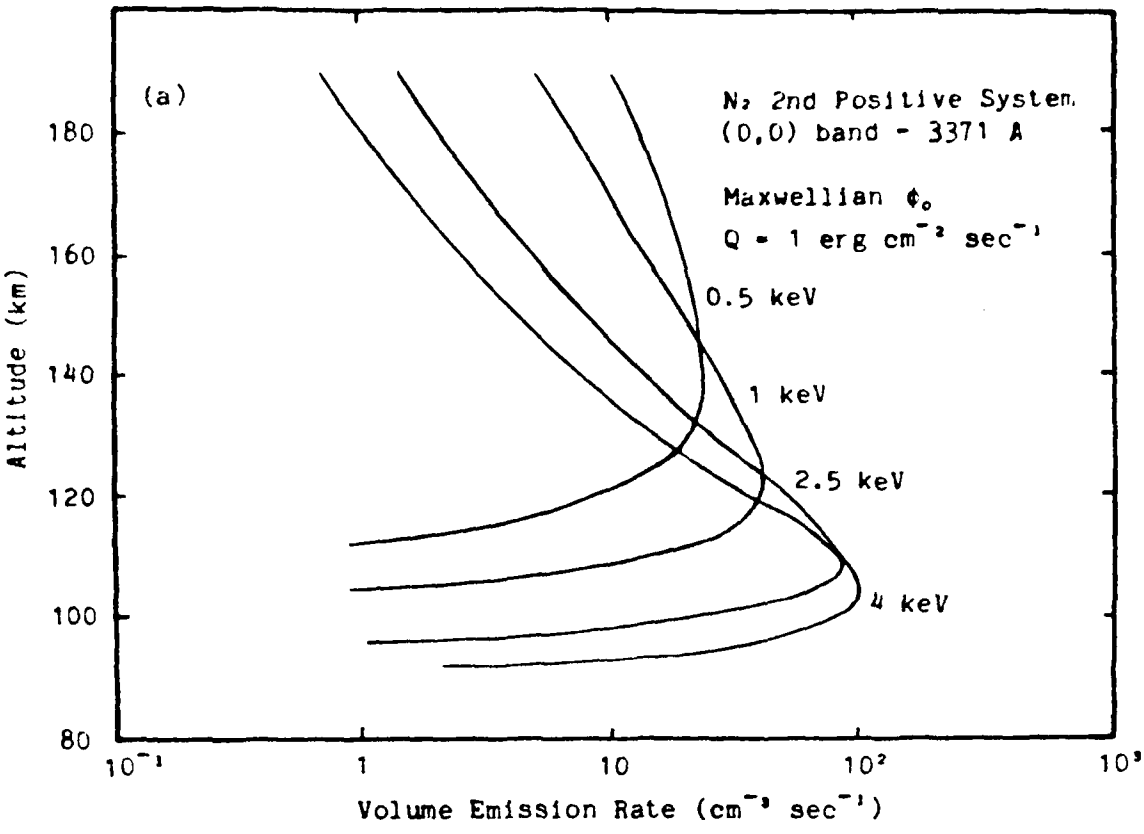

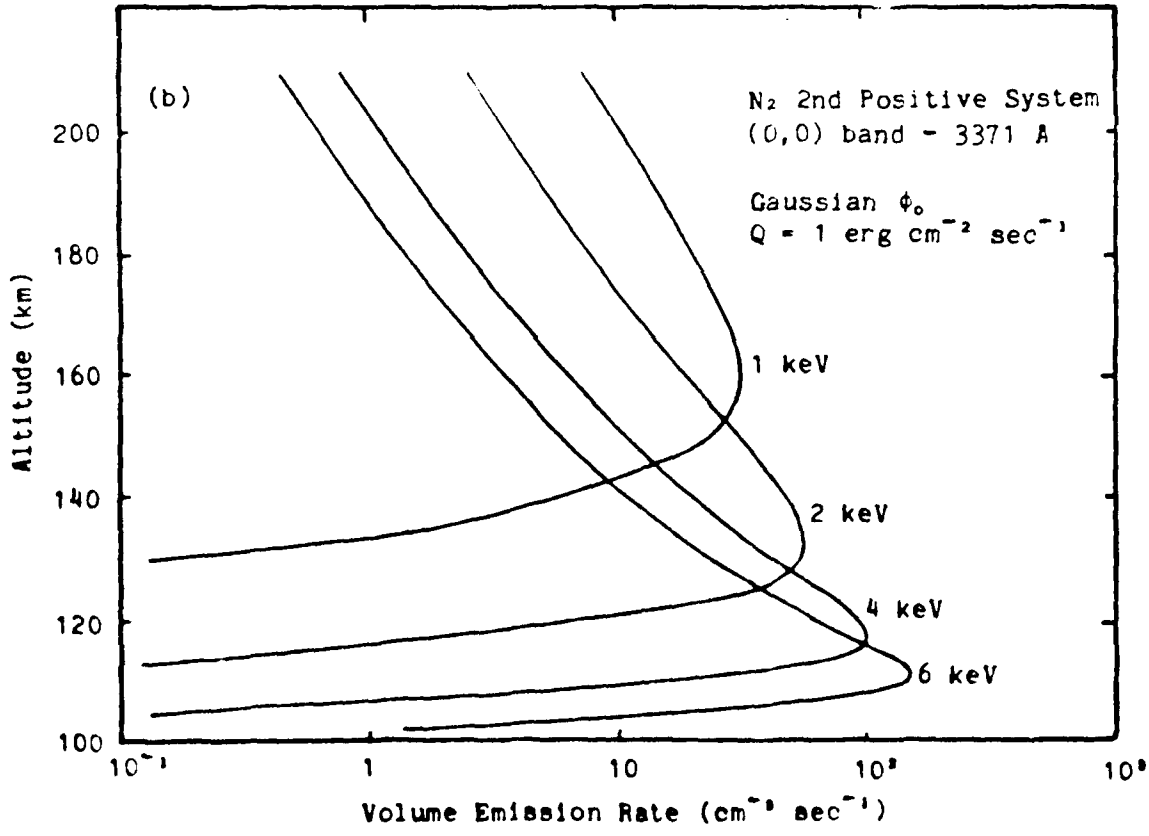

figures 7a and 7b

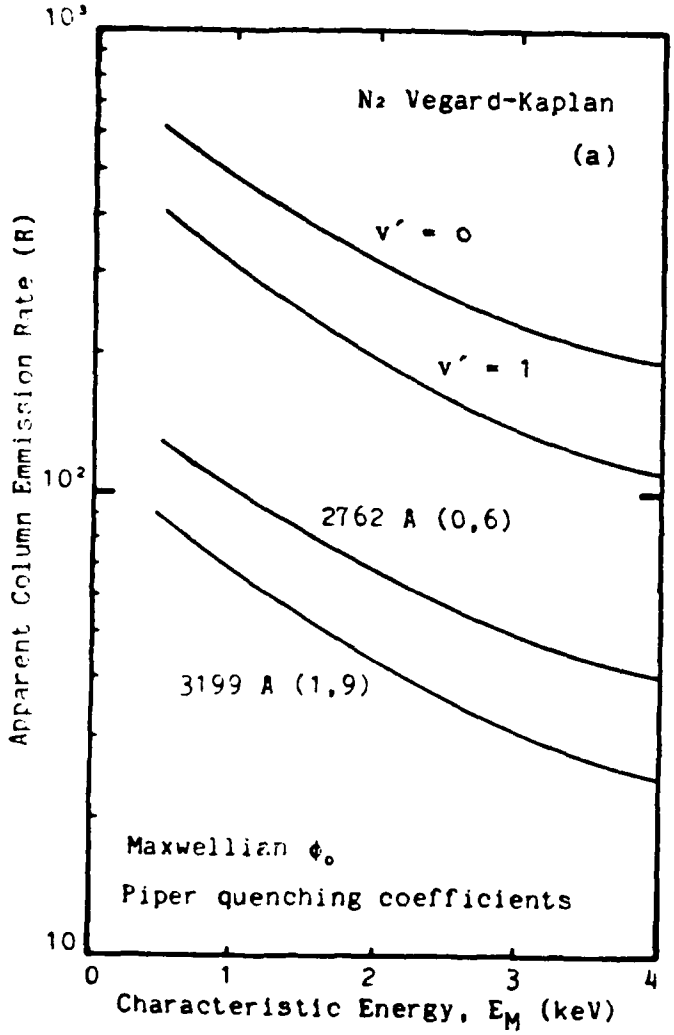

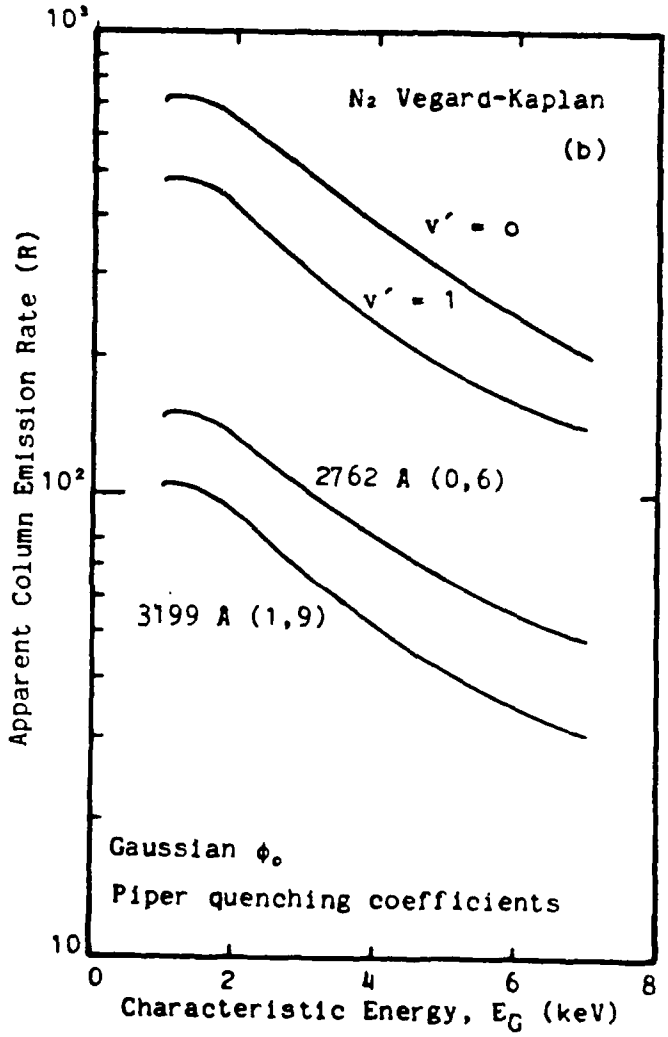

figures 8a and 8b

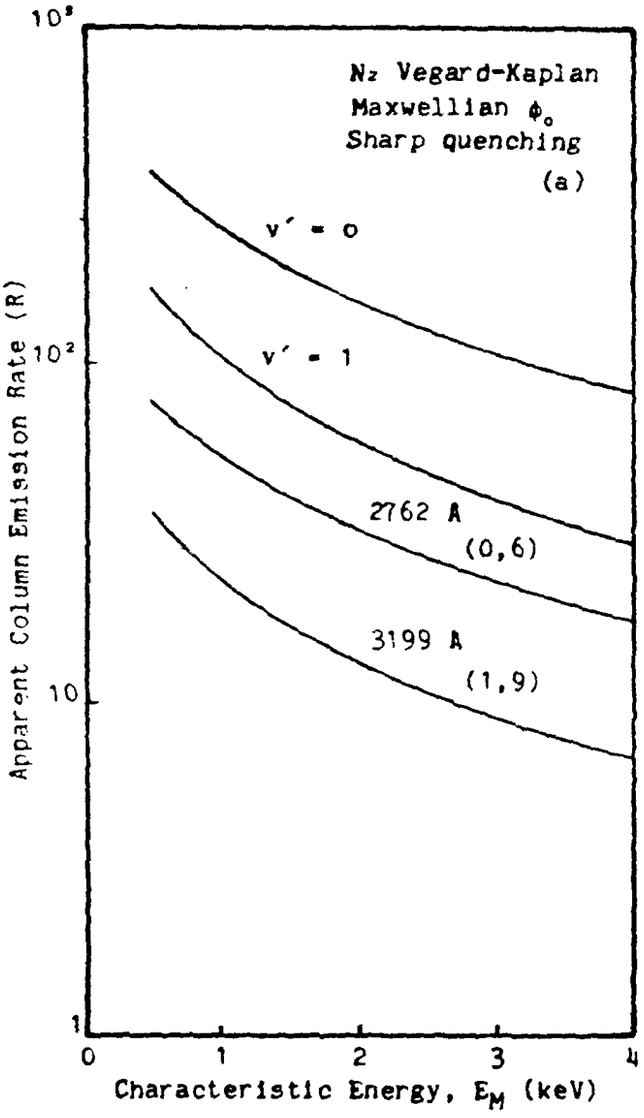

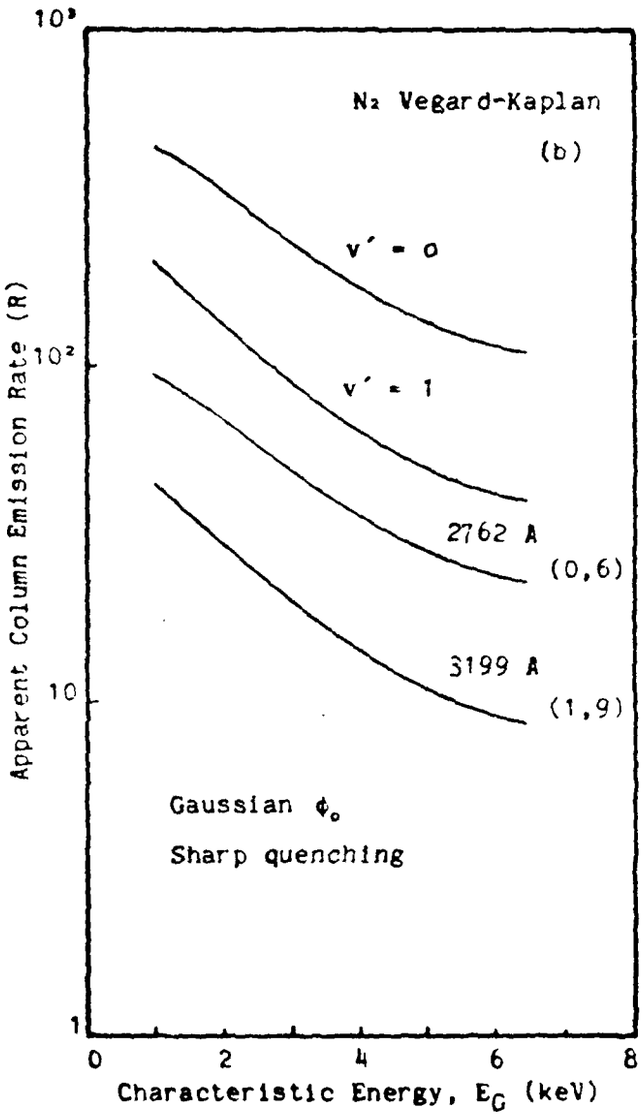

figures 9a and 9b

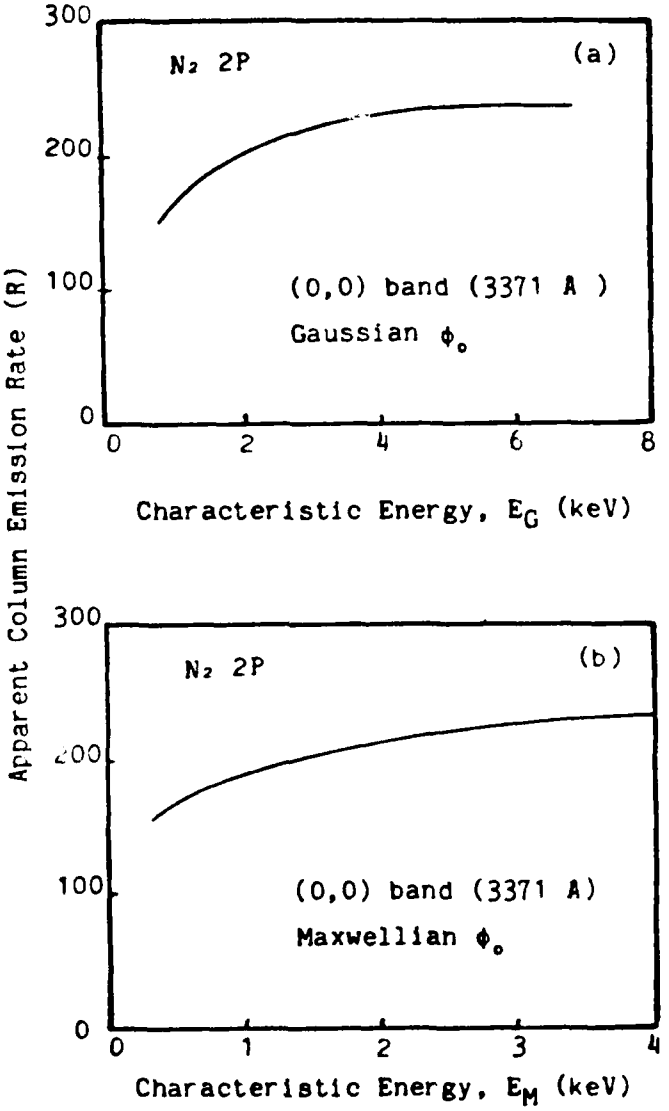

figures 10a and 10b

Appendix B. Using Satellite-Observed UV Intensities to Deduce Electron Density Profiles

by

D. J. Strickland
R. E. Daniell
J. R. Jasperse

(AIAA Journal, Vol. 22, No. 7, pp. 942-947, July 1984)

Using Satellite-Observed uv Intensities to Deduce Electron Density Profiles

D.J. Strickland* and R.E. Daniell†
Beers Associates, Inc., Reston, Virginia

and

J.R. Jasperse‡
Air Force Geophysics Laboratory, Bedford, Massachusetts

This paper addresses the problem of monitoring daytime and auroral ionospheres using optical measurements from satellites. The most attractive approach is to use optical emission features of the neutral atmosphere to monitor both source variability and neutral density and composition. From this information, the electron density profile may be deduced subject to uncertainties caused by neutral winds and electric fields. Emission features, which we examine as candidates for use in this approach, are bands of the N_2 LBH system, N_2 Vegard-Kaplan 2762 Å, N_2^+ 1N 3914 Å, and the atomic oxygen lines at 1356 and 2972 Å. Calculated intensities of these features and n_e are shown for daytime and auroral conditions.

Introduction

IN this paper, we shall discuss work in progress, the goal of which is to assess the utility of satellite-observed optical emission features in deducing the E and F region electron density distributions (n_e). Here we restrict ourselves to the daytime E and F regions and to the auroral E region. We know of no emission feature in these regions that gives a direct signature of the ions present, unlike, say, the O^+ recombination emissions in the tropical nighttime airglow.[1,2] O^+ 834 Å comes closest to fulfilling the requirement since O^+ can affect the 834 Å intensity through multiple scattering.[3] This in itself poses a difficult problem which we shall not address here. It then becomes a two-step process to obtain n_e from optical measurements. We must first obtain a representation of the source (solar ionizing spectrum or incident auroral electron spectrum), followed by its use in calculating n_e. The emphasis in this paper will be on how well the source spectrum can be determined from optical data. To address the second step, we give examples of the sensitivity of n_e to variations in the source spectrum.

The variability of n_e can pose some serious problems for the above technique. This variability is caused by 1) time and spatial changes in the source, 2) the same type of changes in the major neutral density profiles, and 3) mechanics which produce bulk transport of the plasma. As noted above, item 1 shall receive most of our attention. Item 2 is important because uncertainties introduced can affect both the accuracy of the deduced source spectrum and the subsequently calculated n_e profile. The accuracy of n_e is dependent not only on the assumed source spectrum, but also on assumed neutral densities through chemistry and diffusion. More shall be said about item 2 in the third section. Item 3 has to do with winds and fields and will be briefly discussed in the next section. Beyond this, however, we shall restrict ourselves to conditions for which n_e is dependent only on the ionizing source.

We shall examine N_2 LBH 1383 Å and OI 1356 Å in the dayglow. For auroral conditions, we shall consider these as well as OI 2972 Å; the LBH bands at 1273, 1325, and 1354 Å; N_2 Vegard-Kaplan (VK) 2762 Å; and N_2^+ 1N 3914 Å. Some of the auroral results to follow have recently been discussed in more detail in the paper by Strickland et al.[4] In particular, these authors determined the variability of nadir viewing satellite-observed intensities for OI 1356, N_2^+ 3914 Å, and LBH bands at 1273, 1325, and 1383 Å as a function of electron spectral hardness and model atmosphere. The causes of variability in the relative intensities among the above features are variations in 1) excitation efficiencies, 2) pure photon absorption (here due to O_2), and 3) chemical processes (quenching, in particular) that are due to changes in source and neutral atmospheric conditions. Results will follow that demonstrate the strengths of these effects on the emissions.

Ionospheric Variability Due to Neutral Winds and Electric Fields

In the F region ionosphere (above 180 km) both the ion-neutral and electron-neutral collision frequencies are much less than the respective gyrofrequencies. This means that the mobility of a charged particle is much greater along a field line than across field lines. The neutral winds of the thermospheric circulation produce a frictional force on the ionospheric plasma, but only the component of that force which acts along a field line is effective at imparting motion to the plasma. Magnetic field lines lie approximately in meridional planes and rise in altitude toward the equator. During daytime hours, the normal thermospheric circulation is from equator to pole,[5,6] which tends to drive the plasma downward. This reduces not only the altitude of the ionization peak, but also the peak concentration, since chemical losses are larger at lower altitudes. At middle latitudes the effects of these winds can be as important as diffusion, resulting in a lowering of the F_2 peak by ~50 km and a reduction in peak electron density by ~35%.[7,8] However, the thermospheric circulation is quite variable on a daily basis, which makes the ionospheric variability difficult to predict. One source of variability is the energy deposited at high latitudes during geomagnetic substorms which can alter the global thermospheric circulation and even reverse the direction of flow.[6,9] Furthermore, the resistance of ions to cross-field motion can alter the thermospheric winds in the altitude regime above 300 km, further complicating the picture.

In the E region ionosphere (150-160 km) the ion cross-field mobility is considerably larger than that of electrons. In this

Received Jan. 24, 1983; revision submitted Aug. 29, 1983.

*Senior Scientist.
†Scientist.
‡Scientist, Ionospheric Dynamics Branch, Space Physics Division.

altitude regime, neutral winds induce a charge separation which results in a global electric field system. Because magnetic field lines are nearly equipotentials, this electric field system is mapped into the F region, where it causes plasma ($E \times B$) drifts.[7] One may think of the E region winds acting as a dynamo generator while the F region plasma responds as an electric motor. The effect of the electric field is generally smaller than that due to F region winds and varies throughout the day.

In addition to the large-scale effects caused by thermospheric winds and the dynamo electric field, there are small-scale structures—ionospheric irregularities—which have a variety of sources.[7] The irregularities are present in both the E and F regions and at all latitudes.[10,11] At auroral and equatorial latitudes the primary causes of ionospheric irregularities are plasma instabilities, although the relative importance of neutral dynamics in the explanation of equatorial spread F is subject to debate. At midlatitudes, the situation is less well understood. Wind shears are known to produce sporadic E layers while traveling ionospheric disturbances have been explained by gravity waves propagating from below or from the auroral zone. A number of plasma mechanisms have been proposed to explain smaller-scale structures, but verification of these hypotheses awaits more complete sets of observational data.[11]

Both E and F region thermospheric winds can have a significant influence on the electron distribution above 200 km or so. They are hard to observe and continue to be the subject of theoretical and experimental research. If the winds are known, their effects on the ionosphere can be determined.[4] The principal implication for satellite monitoring of the ionosphere is that some method of measuring or calculating thermospheric winds must be developed. Global models of the thermospheric circulation provide a useful beginning, but the effects of geomagnetic activity must also be included if reasonable accuracy is to be obtained. Since ionospheric irregularities are less well understood, particularly at midlatitudes, they present a formidable problem for satellite monitoring. Those problems are not addressed further in this paper, but remain important research subjects.

Emission Variability due to Sources and Neutral Atmosphere

The technique being addressed is most attractive for situations in which the density profiles of N_2, O_2, and O are known. Under those conditions, variability of one optical intensity relative to another with changes in either time or location can be directly related to variability in source conditions. However, the neutral density profiles cannot be precisely known because of their intrinsic variability and the difficulty of precisely describing that variability. The latter problem is due to the approximate nature of existing thermospheric density models (for recent models, see Refs. 12-16) and to the limitations of measurement techniques. Of particular interest here are satellite-based measurements. In situ measurements can be expected to be the most reliable, but may be insufficient for specifying altitude profiles to the degree of accuracy desired. Optical remote sensing techniques, on the other hand, do hold a potential for measuring column densities, which can be used to scale corresponding volume density profiles. This problem is addressed next. One of the objectives of the present work must be to determine just how precisely the major neutral densities need to be known to make the technique under investigation practical. The required precision is dependent on source conditions and, of course, on instrumental conditions.

The problem raised above is whether it is possible to separate the effects of neutral density variations from source variations when using optical data. Various researchers are actively investigating the problem of sensing the neutral atmosphere.[17-19] Their concern has been with the analysis of satellite-observed limb profiles for features such as OI 1356 Å and N_2 LBH bands. We have concentrated our efforts on nadir viewing observations, and we believe that, with the right choice of features and instrumental parameters, the source and atmospheric variabilities can be decoupled. This is strengthened by the fact that there are limitations to the relative variability between the N_2 and O_2 densities in the regions of peak excitation (for either auroral or daytime conditions). Furthermore, the models cited above are probably more than adequate under most observing conditions for describing these relative densities. It then becomes attractive to use selected N_2 band emissions for initially characterizing the source spectrum. For auroral conditions, their relative strengths indicate the hardness of the electron source spectrum through either of the basic mechanisms of pure absorption or quenching, depending on the features. Given a representation of the spectral hardness, the magnitudes of the observed intensities then determine the energy content of the spectrum. In the daytime ionosphere, most of the F region ionization is produced by radiation in the range 100-800 Å with a smaller contribution from the 800-910 Å range.[8] The radiation below 150 Å produces only 5 to 8% of the ionization, depending on solar activity. Since the shape of the solar spectrum in the wavelength range 150-910 Å does not vary drastically with solar activity,[8] the important parameter is the energy content of that part of the spectrum. The magnitudes of the observed airglow intensities provide a measure of that parameter. However, the variability of the ultraviolet dayglow is not well understood. Rocket data analyzed by Meier et al. (Ref. 20 and personal communication) indicate that the variability is weaker than the results presented below would suggest. This remains an area of active investigation.

With an initial characterization of the source spectrum, we may turn to the problem of better determining the neutral densities. The atomic oxygen density is of prime interest, since it probably experiences the greatest relative variation (see above papers on thermospheric modeling) and has associated with it some key uv emission features (examples are OI 1304 Å, OI 1356 Å, and OI 2972 Å). Because O is a minor species when considered over the entire excitation region, its optical intensities are sensitive to its overall density. Thus, given the source spectrum, a measure of, say, the OI 1356 Å intensity (with a minor contamination from N_2 LBH 1354 Å) gives a direct measure of the magnitude of the O density profile. We may now repeat the process to further improve both the source representation and neutral density description.

Computational Models

Daytime Ionosphere

We possess two models and associated computer codes for describing the interactions of solar ionizing radiation and photoelectrons with the atmosphere. One is the Boltzmann-Fokker-Planck model of Jasperse,[21,22] which provides detailed energy spectra of the electrons over both the thermal and photoelectron energy regions. The other model is by Strickland and Meier,[23] and also gives photoelectron spectra, but with a less detailed description of the Boltzmann collision integral. In the second model, more emphasis is placed on the calculation of optical intensities. Chemistry codes are coupled to the abovementioned photoelectron codes to calculate temperatures, ion densities, and various neutral densities. Results to follow will come from the use of the second photoelectron model mentioned above and associated chemistry code which allows for O^+ diffusion.

Auroral Ionosphere

The electron transport model of Strickland et al.[24] is used to specify the electron spectrum and associated excitation and ionization rates. A Boltzmann equation is solved which gives the spectrum or distribution function from the highest primary energy of interest down to the eV range. Electron interactions

are limited to the particle-particle type, which includes elastic scattering, excitation, and ionization leading to energy loss of the incident electron and production of a secondary electron. A time-dependent chemistry code is coupled to the transport results and gives the densities of numerous ions and neutrals, along with intensities for a variety of emission features. This code is essentially the same as the one from which the daytime results to follow were obtained.

Comparisons with Optical, Electron, and Ion Data

The calculation of photoelectron and auroral electron spectra, excitation rates, chemical species, densities, and optical intensities involves a large body of input data and the use of some large computer codes. It is essential to compare these calculated quantities with independent results as well as measurements prior to a serious investigation of the problem being addressed. Three such comparisons follow.

We first note that electron spectra are the most difficult to calculate the abovementioned quantities. We have tested them through various comparisons and by observing how well they conserve energy. The latter test typically yields an error of less than 10%. The auroral electron results have been well tested, beginning with comparisons discussed by Strickland et al.[4] followed by subsequent comparisons with rocket and satellite data. This latter work is unpublished but does generally show good agreement. Specific examples of applied data are the rocket data of Spiger and Anderson[25] and satellite data of Craven and Frank.[26] The observed quantity is the auroral electron spectrum given as a function of both energy and angle. With regard to the calculated photoelectron spectra, excellent agreement has been achieved with both data and independent calculations. These comparisons may be seen in the report of Strickland and Meier.[23]

For the comparisons to follow, we have chosen optical, ion density, and electron density data, since these are the types of data we are ultimately interested in. We begin with the electron density information in Fig. 1, which comes from Jasperse.[22] This figure shows good overall agreement between theory and experiment for daytime conditions. An example of fractional ion abundances under auroral conditions is shown in Fig. 2. The data come from Swider and Narcisi[28] and were obtained with an ion mass spectrometer mounted on a rocket fired into the continuous aurora. The calculated results show good overall agreement, with the exception of those for N_2^+ which lie above the data. For this same experiment, satisfactory agreement was also obtained between the calculated electron density and coincident radar data. As an example of a comparison with optical data, we show in Fig. 3 results from Strickland and Anderson[29] which give the 1356 Å limb intensity for daytime conditions. The data were provided by Newman and Christensen from a spectrometer experiment on board satellite DMSP-F4.[17,19] Calculations of the needed photoelectron spectra and excitation rates come from the second of the previously discussed photoelectron models,[23] while the remaining calculations were provided by the photon transport model of Anderson et al.[30]

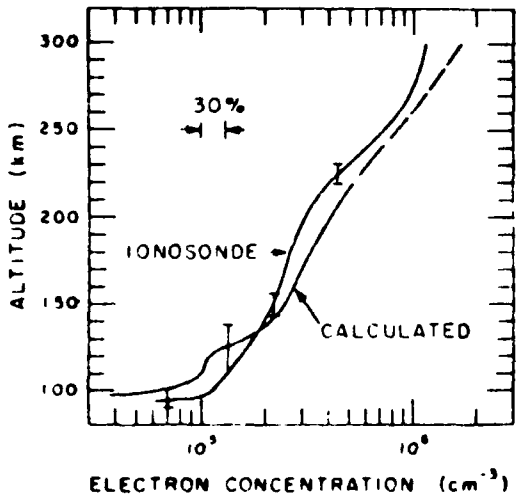

Fig. 1 Calculated and observed[27] electron concentration vs altitude. The estimated errors given for the ionosonde measurement are 0 to +30 km near 120 km and ±5 km elsewhere. Calculated concentrations above 220 km shown as dotted curve. Solar zenith angle was 27 deg.

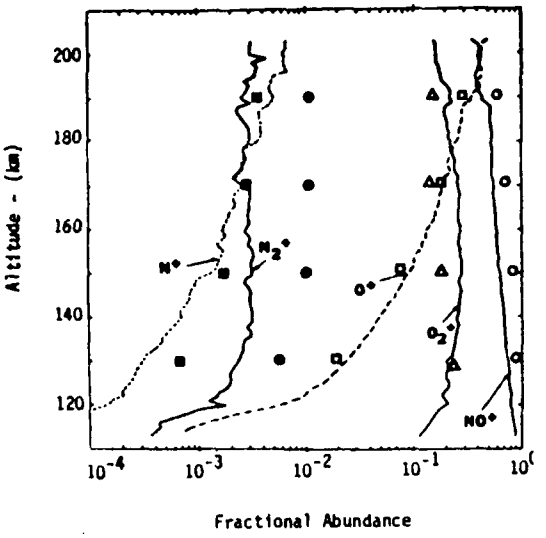

Fig. 2 Fractional ion abundances for the continuous aurora. Data are given by the solid and broken curves and come from Swider and Narcisi.[28]

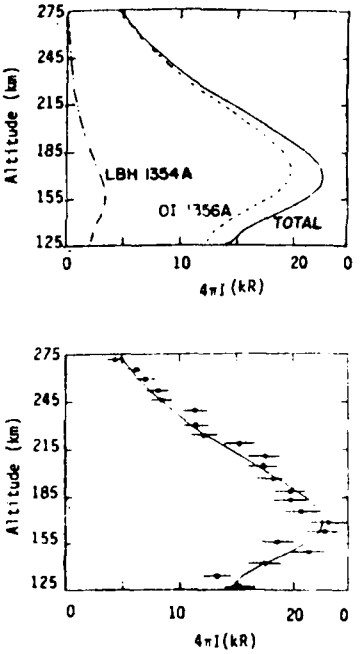

Fig. 3 1356 Å dayglow limb intensity. Data are from Newman and Christensen[17,19] while calculations are from Strickland and Anderson.[29]

Daytime Results

In this section, we wish to demonstrate the variability of optical emissions and n_e caused by changes in the solar

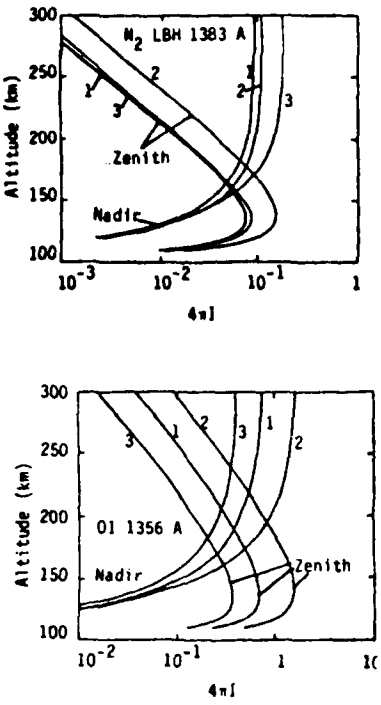

Fig. 4 Zenith and nadir viewing OI 1356 Å and N_2 LBH 1383 Å dayglow intensities. The solar zenith angle is 60 deg. The labeling refers to the following conditions: 1) low solar activity, Jacchia 1977 $n(0)$; 2) high solar activity, Jacchia 1977 $n(0)$; 3) low solar activity, half of Jacchia 1977 $n(0)$.

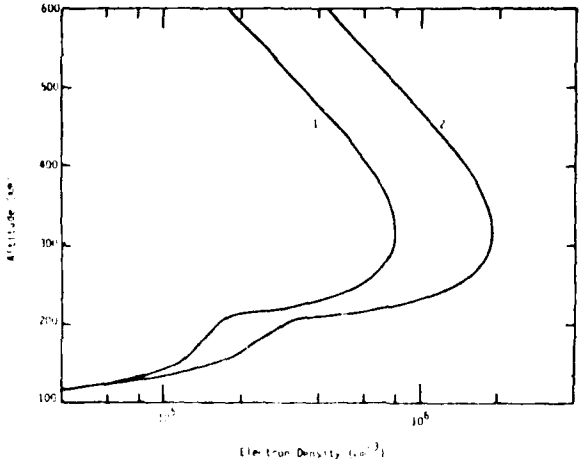

Fig. 5 Calculated daytime electron density. Labeling is the same as in Fig. 4.

activity and the neutral densities. We have just begun addressing this problem and will restrict the results to two key optical features and three starting conditions. The features to be considered are LBH 1383 Å [the (2,0) and (5,2) bands] and OI 1356 Å. Both features are at sufficiently short wavelengths that Rayleigh scattering of solar radiation does not contaminate their intensities on emerging from the ionosphere. Conditions are defined in terms of solar activity (indexed by $F_{10.7}$, the 10.7 cm solar flux) and the model atmosphere. We use solar spectrum representations from Torr et al.[31] for high ($F_{10.7} = 207$) and low ($F_{10.7} = 71$) activity. The basic model atmosphere comes from the 1977 Jacchia model.[12] One set of results will be shown for which the O density has been reduced by half.

Figure 4 shows nadir and zenith viewing intensities for the three sets of starting conditions. We observe a change in intensity of ~ 2 in going from low to high solar activity. As expected, halving the atomic oxygen density reduces the OI 1356 Å intensity by a similar factor. The LBH 1383 Å intensity is altered only slightly because of a small reapportionment of photoelectron energy received by N_2. As we mentioned above, the actual variation in OI 1356 Å due to solar variability may be less than our calculations indicate. If so, it may be that the Torr et al.[31] solar spectra overestimate the amount of euv variability. This problem remains under investigation.

Figure 5 shows electron densities for the two levels of solar activity. The results above 200 km include the effect of diffusion. We regard these results as preliminary, since they are the first we have obtained for daytime conditions and since the diffusion model is still under development. Although they are preliminary, the results for the two sets of conditions are sufficient for demonstrating the variability in the electron density profile and its relationship to corresponding variability in optical intensities.

Nighttime Auroral Results

In the previous section, we observed that changes in source conditions (changes in solar activity) lead to changes in emission brightness without noticeably affecting relative emission strengths. It is, thus, the absolute intensities of optical features that concern us in the daytime ionosphere with regard to monitoring variations in the source spectrum. The situation is noticeably different in the auroral ionosphere, where a wide range of altitude profiles can exist in volume excitation and emission rates due to variability in the hardness of the incident electron spectrum. This leads to some significant variations in relative intensities, since changes in the above altitude profiles affect excitation efficiencies and the extent to which pure absorption and quenching operate. We shall now examine such variations for the purpose of determining how well one can hope to characterize the source spectrum from optical measurements.

Intensities have been calculated for viewing in the nadir direction from above the emitting region. The incident spectrum is described by a Maxwellian distribution having the form

$$\phi_0(E,\mu) = \left(\frac{Q_M}{2\pi E_M^3}\right) E\exp(-E/E_M)\,\mathrm{e/cm^2\text{-}s\text{-}eV\text{-}sr}$$

where E and μ are, respectively, the electron energy and cosine of the pitch angle, E_M is the characteristic energy, and Q_M is the energy flux. Calculations have been performed for $Q_M = 1$ erg/cm^2-s and for E_M values over the range from 0.5 to 5 keV. Figures 6a and 6b show the calculated intensities of the features under consideration as functions of E_M. A Jacchia 1977 model atmosphere was used for all calculations. We observe varying amounts of decrease for all features except N_2^+ 3914 and LBH 1273 Å. The decreases in Fig. 6a are caused primarily by the increasing amount of O_2 pure absorption. Some of the decrease at 1356 Å is also caused by a decreasing excitation efficiency for atomic oxygen. Pure absorption has little effect at 1273 or 3914 Å, or at the wavelengths considered in Fig. 6b. The decreases exhibited at 2762 and 2972 Å are caused primarily by quenching. Some of the decrease at 2972 Å, as at 1356 Å, is also caused by a decreasing excitation efficiency. The states from which these emissions arise are $N_2(A\,^3\Sigma)$ and $O(^1S)$, which are coupled in the sense that an important source of ^1S excitation comes from the reaction

$$N_2(A) + O \rightarrow N_2(X) + O(^1S)$$

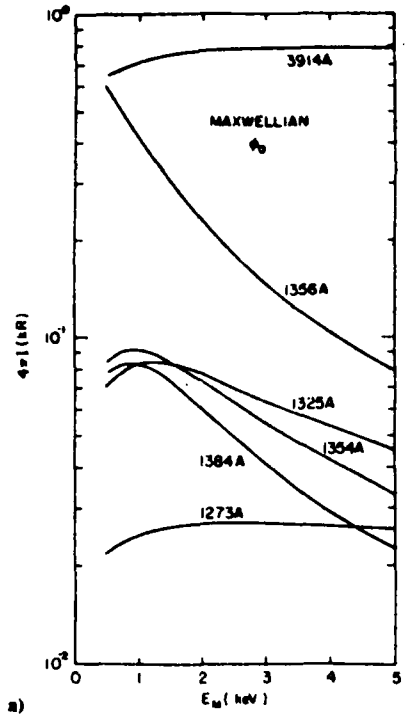

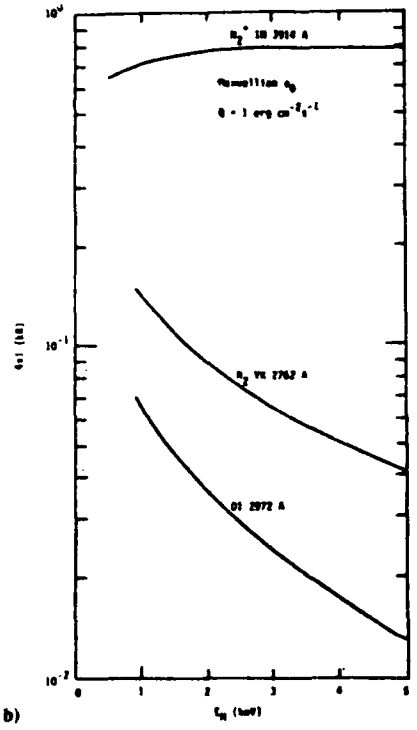

Fig. 6 Nadir viewing auroral intensities as functions of the incident electron spectrum. Spectra are represented by Maxwellian distributions where E_M is the Maxwellian characteristic energy.

The more prominent emission from the ^1S state is at 5577 Å, which we have excluded because its nadir-observed intensity is contaminated by emission and scattering below the ionosphere. The 3914 Å intensity will also be affected by scattering and albedo, but in spite of this we include it in Fig. 6 since it is one of the most prominent and frequently observed uv features in the aurora.

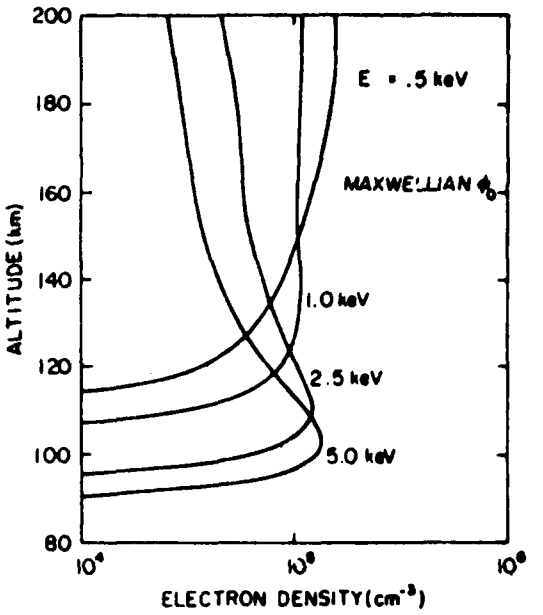

Fig. 7 Auroral E region electron densities for four different incident electron spectra represented by Maxwellian distributions.

We have obtained profiles similar to those shown in Fig. 6 for other model atmospheres. In particular, we have scaled the O_2 and O densities in various ways to generate these models. As expected, the most notable changes have come from scaling the O density. The OI 1356 Å intensity varies nearly directly with the O scaling factor because the main source is direct excitation of $O(^5S)$ with a small contribution (~ 10%) from dissociative excitation of O_2. Little effect is observed in the N_2 emissions. Thus, this intensity is potentially valuable for monitoring either source conditions or the O density, depending on how well these are known from independent information. We should note that multiple scattering of the 1356 Å photons does occur, but has only a minor effect for the given viewing conditions.[29,30]

The final results we wish to consider are electron densities and, in particular, the sensitivity of their altitude profiles to changes in the source spectrum. Figure 7 illustrates this sensitivity in which we show four profiles for characteristic energies of 0.5, 1, 2.5, and 5 keV. Since most of our attention until recently has been directed to the auroral E region, we choose here to limit our discussion to the behavior of n_e under chemical equilibrium conditions. For all results, $Q_M = 1$ erg/cm^2-s as before. We do observe noticeable changes in the n_e profiles shown, although not in maximum values. It is worth comparing results such as these to results for other types of source representations. We have done so by carrying out a series of calculations for incident electron spectra characterized by narrow Gaussian distributions.[4] We find the overall profile to be similar where respective characteristic energies are chosen to give the same altitude of maximum ionization. For the more nearly monoenergetic Gaussian source, however, n_e peaks somewhat more sharply and does not penetrate as deeply into the atmosphere.

Much more can be said about the results presented in this section. We have limited the discussion, in part because details are available elsewhere,[4] and our emphasis is meant to be on the larger picture of just how much potential optical observations hold for monitoring the ionosphere. We complete this paper in the next section with some general comments at this level of consideration.

Discussion

Clearly, we have not answered the question of just how effectively n_e and the major neutral densities, especially $n(0)$,

can be monitored by optical techniques. This is a difficult question which first requires statements of the needed accuracy in the deduced quantities and of instrument capability. Given this information, we can then proceed to incorporate results of the type discussed in this paper into a statistical analysis, out of which come deduced density profiles with associated standard deviations for specific optical data sets. This should be done initially under ideal conditions, which means that these deviations would not reflect uncertainties introduced by winds and fields.

What we are able to say at this time is that selected uv features do show sufficient variability in their intensities to make it worthwhile to proceed with the kind of analysis discussed above. We shall be continuing our investigation along these lines with an important part of this work directed to those complications which remove us from ideal modeling conditions. Among such complications not previously mentioned are the nonanalytic nature of actual auroral electron spectra and incomplete spectroscopic information (see, e.g., Refs. 32 and 33).

Acknowledgments

This work was partially sponsored by the DMSP Program Office, Space Division, Air Force Systems Command.

References

[1]Chandra, S., Reed, E.I., Meier, R.R., Opal, C.B., and Hicks, G.T., "Remote Sensing of the Ionospheric F Layer by Use of OI 6300 Å and OI 1356 Å Observations," *Journal of Geophysical Research*, Vol. 80, No. 16, 1975, pp. 2327-2332.

[2]Tinsley, B.A. and Bittencourt, J.A., "Determination of the F Region Height and Peak Electron Density at Night Using Airglow Emissions from Atomic Oxygen," *Journal of Geophysical Research*, Vol. 80, No. 16, 1975, pp. 2333-2337.

[3]Feldman, P.D., Anderson, D.E., Jr., Meier, R.R., and Gentieu, E.P., "The Ultraviolet Dayglow 4. The Spectrum and Excitation of Singly Ionized Oxygen," *Journal of Geophysical Research*, Vol. 86, No. A5, 1981, pp. 3583-3588.

[4]Strickland, D.J., Jasperse, J.R., and Whalen, J.A., "Dependence of Auroral FUV Emissions on the Incident Electron Spectrum and Neutral Atmosphere," *Journal of Geophysical Research*, 1983, in press.

[5]Bauer, S.J., *Physics of Planetary Ionospheres*, Springer-Verlag, New York, 1973, pp. 185-189.

[6]Evans, J.V., "The Dynamics of the Ionosphere and Upper Atmosphere," in *Physics of Solar Planetary Environment*, American Geophysical Union, Washington D.C., 1976, pp. 630-671.

[7]Hargreaves, J.K., *The Upper Atmosphere and Solar Terrestrial Relations*, Van Nostrand Reinhold, New York, 1979, pp. 72-74.

[8]Banks, P.M. and Kockarts, G., *Aeronomy*, Academic Press, New York, 1973, pp. 169-190.

[9]Prolss, G.W., "Perturbation of the Low-Latitude Upper Atmosphere During Magnetic Substorm Activity," *Journal of Geophysical Research*, Vol. 87, No. A7, 1982, pp. 5260-5266.

[10]Ossakow, S.L., "Ionospheric Irregularities," *Reviews of Geophysics and Space Physics*, Vol. 17, No. 4, 1979, pp. 521-533.

[11]Fejer, B.G. and Kelley, M.C., "Ionospheric Irregularities," *Reviews of Geophysics and Space Physics*, Vol. 18, No. 2, 1980, pp. 401-454.

[12]Jacchia, L.G., "Thermospheric Temperature, Density, and Composition: New Models," *Spec. Rep.*, 375, Smithsonian Astrophysical Observatory, Cambridge, Mass. 1977.

[13]Hedin, A.E., Salah, J.E., Evans, J.V., Reber, C.A., Newton, G.P., Spencer, N.W., Kayser, P.C., Alcayde, D., Bauer, P., Cogger, L., and McClure, J.P., "A Global Thermospheric Model Based on Mass Spectrometer and Incoherent Scatter Data, MSIS 1, N_2 Density and Temperature," *Journal of Geophysical Research*, Vol. 82, No. 16, 1977, pp. 2139-2147.

[14]Hedin, A.E., Reber, C.A., Newton, G.P., Spencer, N.W., Brinton, H.C., Mayr, H.G. and Potter, W.E., "A Global Thermospheric Model Based on Mass Spectrometer and Incoherent Scatter Data, MSIS 2, Composition," *Journal of Geophysical Research*, Vol. 82, No. 16, 1977, pp. 2148-2156.

[15]Barlier, F., Berger, C., Falin, J.L., Kockarts, G., and Thuillier, G., "A Thermospheric Model Based on Satellite Drag Data," *Annals of Geophysics*, Vol. 34, 1978, pp. 9-24.

[16]Hedin, A.E., Spencer, N.W., Mayr, H.G., and Porter, H.S., "Semi-empirical Modeling of Thermospheric Magnetic Storms," *Journal of Geophysical Research*, Vol. 86, No. A5, 1981, pp. 3515-3518.

[17]Newman, A.L., Christensen, A.B., and Anderson, D.E., Jr., "Atomic Oxygen Density Deduced From Limb-Scans of the UV Dayglow," *Journal of Geophysical Research*, Vol. 88, No. A11, 1983, pp. 9265-9270.

[18]Meier, R.R. and Anderson, D.E., Jr., "Determination of Atmospheric Composition and Temperature from the UV Airglow," *Planetary and Space Sciences*, Vol. 31, 1983.

[19]Christensen, A.B., Newman, A.L., and Anderson, D.E., Jr., "Results of a Satellite-Borne Limb Scanning UV Spectrometer From Remote Sensing of Atmospheric Density," *21st* Aerospace Sciences Meeting, Reno, Nev., Jan. 1983.

[20]Meier, R.R., Strickland, D.J., Feldman, P.D., and Gentieu, E.P., "The Ultraviolet Dayglow, 1. Far UV Emissions of N and N_2," *Journal of Geophysical Research*, Vol. 85, May 1982, pp. 2177-2184.

[21]Jasperse, J.R., "Boltzmann-Fokker-Planck Model for the Electron Distribution Function in the Earth's Ionosphere," *Planetary and Space Sciences*, Vol. 24, 1976, pp. 33-40.

[22]Jasperse, J.R., "Electron Distribution Function and Ion Concentrations in the Earth's Lower Ionosphere From Boltzmann-Fokker-Planck Theory," *Planetary and Space Sciences*, Vol. 25, 1977, pp. 743-756.

[23]Strickland, D.J. and Meier, R.R., "A Photoelectron Model for the Rapid Computation of Atmospheric Excitation Rates," National Research Laboratories Memorandum Report 5004, 1982.

[24]Strickland, D.J., Book, D.L., Coffey, T.P., and Fedder, J.A., "Transport Equation Techniques for the Deposition of Auroral Electrons," *Journal of Geophysical Research*, Vol. 81, No. 16, 1976, pp. 2755-2764.

[25]Spiger, R.J., and Anderson, H.R., "Electron Currents Associated with an Auroral Band," *Journal of Geophysical Research*, Vol. 80, No. 16, 1975, pp. 2161-2164.

[26]Craven, J.D. and Frank, L.A., "Electron Angular Distributions Above the Day Side Auroral Oval," *Journal of Geophysical Research*, Vol. 81, No. 10, 1976, pp. 1695-1699.

[27]Neroux, L., Cohen, M., and Higgens, J.E., "Electron Densities Between 110 and 300 km Derived from Solar EUV Fluxes of August 23, 1972," *Journal of Geophysical Research*, Vol. 79, No. 34, 1974, pp. 5237-5244.

[28]Swider, W. and Narcisi, R.J., "Problems with the $N_2^+ + O \rightarrow NO^+ + N$ Reaction in Aurora," *Geophysical Research Letters*, Vol. 8, No. 12, 1981, pp. 1239-1241.

[29]Strickland, D.J. and Anderson, D.E., Jr., "Radiation Transport Effects on the 1356 Å Limit Intensity Profile in the Dayglow," *Journal of Geophysical Research*, Vol. 88, No. A11, 1983, pp. 9260-9264.

[30]Anderson, D.E., Jr., Meier, R.R., Feldman, P.D., and Gentieu, E.P., The UV Dayglow 3. OI Emissions at 989, 1027, 1304, and 1356 Å," *Geophysical Research Letters*, Vol. 7, No. 12, 1980, pp. 1057-1060.

[31]Torr, M.R., Torr, D.G., Ong, R.A., and Hinteregger, H.E., "Ionization Frequencies for Major Thermospheric Constituents as a Function of Solar Cycle 21," *Geophysical Research Letters*, Vol. 6, No. 10, 1979, pp. 711-744.

[32]Huffman, R.E., LeBlanc, F.J., Larrabee, J.C., and Paulson, D.E., "Satellite Vacuum Ultraviolet Airglow and Auroral Observations," *Journal of Geophysical Research*, Vol. 85, No. A5, 1980, pp. 2201-2215.

[33]McLaughlin, R.W., Erdman, P.W., and Zipf, E.C., "On the Excitation of the N_2 LBH System in the Airglow and Aurora," *EOS, Transactions, American Geophysical Union*, Vol. 63, No. 18, 1982, p. 394.

Appendix C. Global Monitoring of the Ionosphere by Optical Techniques

by

R. E Daniell, Jr.
D. J. Strickland
J. R. Jasperse

(presented at the 1984 Ionospheric Effects
Symposium, Alexandria, VA, May 1-3)

GLOBAL MONITORING OF THE IONOSPHERE BY OPTICAL TECHNIQUES

R.E. Daniell, Jr. and D.J. Strickland
Beers Associates, Inc.
Post Office Box 2549
Reston, VA. 22090

J.R. Jasperse
Air Force Geophysics Laboratory
Hanscom Air Force Base, MA. 01731

ABSTRACT

This paper presents a progress report on our efforts toward determining the feasibility of monitoring the global ionosphere using satellite observations of auroral and airglow optical emissions. After giving an overview of our approach, we concentrate on the nighttime midlatitude ionosphere for which the most straightforward methods are applicable. There are several atomic oxygen emission features which are directly related to ionospheric parameters. Our analysis indicates that the OI 1356 A feature can be monitored by existing photometer technology. This feature provides a direct measure of the peak electron density and total electron content. The OI 6300 A feature can be used to monitor the height of the peak, but a large background signal must be measured and subtracted. Our analysis indicates that a state-of-the-art tilting filter photometer can be used for this purpose. However, since no instrument comparable to the one we propose has ever been flown on a satellite, a dedicated proof-of-principle experiment should be performed. The dayside and auroral ionospheres have no comparable features which provide direct measures of the electron density. However, there are several emission features which respond to changes in the source and/or the neutral atmosphere. We show synthetic spectra which illustrate this variability and briefly discuss the usefullness of some of these features.

1. INTRODUCTION

In this paper, we address the problem of remote optical sensing of the electron density profile, n_e, on a global scale. We specifically apply a nighttime model to a highly dynamic situation and also show the kinds of UV spectral variability to be expected in the auroral and daytime ionospheres for nadir viewing from a satellite. In the nighttime ionosphere, the optical emissions of interest arise from various chemical processes starting with the loss of O^+ by either recombination or charge exchange. Features which we single out here are OI 1356 A and OI 6300 A. The model discussed in Section 3 shows how these features may be used to directly deduce n_e. In the auroral and daytime ionospheres, the optical emissions of interest arise from the interaction of secondary and primary electrons with neutrals. Features which we single out here are N_2 LBH bands and OI 1356 A. UV spectra containing these and other features vary with the source and neutral atmosphere and therefore convey information about these quantities. This information may be used to specify n_e with appropriate models. Key issues here are 1) how well source and neutral density information may be specified from satellite observed optical emissions and 2) how accurately n_e may be deduced once given this information. Ultimately, these questions must be answered with a dedicated experimental program. In the meantime, we define as best we can the relationship between n_e and UV spectra using first principles models and available relevant data.

Most of this paper addresses the nighttime midlatitude ionosphere. For orientation, we list the sources of uncertainty affecting n_e as deduced from optical data. They are 1) calibration, 2) counting statistics, 3) dark counts, 4) background, and 5) the applied model. The model introduces uncertainty through 1) an assumed shape for n_e (Chapman function), 2) an assumed exospheric temperature, 3) applied rate coefficients, and 4) assuming O^+ to be the only ion on the top side (ignoring increasing importance of H^+ with increasing altitude). These various uncertainties will be discussed in later sections.

2. BACKGROUND

Over the past few years, we have been investigating the relationship between UV emissions and the electron density profile, $n_e(z)$. Much of this effort has been directed to the continuous aurora (Strickland et al., 1983). Recently, we have turned our attention to the midlatitude nighttime ionosphere and the low to midlatitude daytime ionosphere. (Strickland et al. 1984). Our long term interest is to establish the effectiveness of satellite near-nadir UV data for monitoring $n_e(z)$ from the E region to the upper F region under quiescent plasma conditions. A parallel effort is under way by R.R. Meier and colleagues at the Naval Research Laboratory. To date, their emphasis has been on establishing the usefullness of UV limb intensity profiles for monitoring the major neutral constituents (N_2, O_2, and O), exosphere temperature, and excitation sources (solar EUV spectrum and incident auroral electron spectrum; see, e.g. Meier and Anderson, 1984 and Meier et al., 1982). The NRL program effectively compliments our own, the latter being under Air Force sponsorship.

Our program is a combination of 1) investigating basic mechanisms, 2) determining what can be learned from existing satellite, rocket, and ground based data, and 3) directing attention to systems aspects of the problem such as instrument definition and operational requirements. The investigation of basic mechanisms has been done with first priciples models applied to the auroral and daytime ionospheres. Here, we begin with a source spectrum (energetic incident auroral electrons or a solar EUV and X-ray spectrum) and model neutral density atmosphere. The electron density and numerous UV intensities are then calculated using transport and chemistry algorithms within these first principles models. These results are examined to determine patterns of change with changes in input parameters and are also compared with data when available. Most of our efforts have been directed to the E and lower F regions. We are now beginning to actively investigate how well n_e can be determined at higher altitudes using a combination of UV data, in situ measurements at satellite altitudes, and present knowledge of F-region dynamics. A key to using the optical techniques on the auroral and daytime ionospheres is UV spectral variability. Examples of this variability will be given in Sections 7 and 9 in the form of synthetic spectra.

Regarding item 2), our primary interest is in those situations where n_e and UV emissions are being simultaneously monitored. Unfortunately, such situations are rare and generally were not intended for correlating these observations (rocket experiments are the exception and are mentioned below). Thus, we find ourselves searching, e.g., for ground based ionosonde or radar data coincident with satellite UV data such as those obtained on OGO-4 (Barth and Schaffner, 1970; Sharp and Rees, 1972; Prinz and Meier, 1971), STP 72-1 (Anderson et al., 1976), P78-1 (Chakrabarti et al., 1983; Paresce et al., 1983), and S3-4 (Huffman et al., 1980). Such searches have been done with limited success in the nighttime ionosphere (Meier and Opal, 1973; Chandra et al., 1975). We are not aware of successful searches in either the auroral or daytime ionospheres.

There have been rocket experiments providing the opportunity to correlate n_e and UV data. In some cases, n_e was obtained by rocket instrumentation and in others from the ground by ionosonde or radar. Examples of auroral experiments are a March 1974 experiment reported by Rees et al. (1977) and Sharp et al. (1979) and a March 1981 experiment largely unreported to date (see Swider and Narcisi, 1981 for ion data). We have compared calculated n_e and UV intensities with data from both experiments and have found generally good agreement (< 30% differences over most of the observed altitude range). An example of a daytime experiment is one in January, 1978 reported by Gentieu et al. (1979) and Meier et al. (1980). In this case, n_e was obtained from ground based ionosonde data but has not been reported in the literature. The UV optical data are well understood (Meier et al., 1980) and we are now in the process of comparing calculated n_e values with the measured ones.

As noted above, there are a limited number of opportunities to examine n_e and UV optical data obtained at the same time and location. Ultimately, an experimental program must be undertaken using a satellite and an array of ground stations for obtaining these quantities in order to effectively test the UV remote sensing technique. Until then, the best we can do is to continue improving our understanding of basic mechanisms through modeling and analysis of existing data even though they generally form an incomplete set in terms of sources, neutral and charged particle densities, and optical emissions.

Regarding item 3), much of our attention has been directed to instrumentation for observing the nightglow. The challenge here is to achieve the necessary sensitivity for monitoring emission rates at the sub-Rayleigh level and the necessary wavelength resolution to provide the needed information for subtracting backgrounds. Photometers and spectrometers are both being assessed for their effectiveness on the one hand to monitor the weak nightglow emissions while on the other to monitor the much brighter emissions in the auroral and daytime ionospheres.

3. APPLIED NIGHTTIME MODEL

Optical techniques for monitoring the n_e are particularly attractive when applied to the nighttime midlatitude ionosphere. Here, emissions are direct signatures of the height and magnitude of n_e. These emissions come from radiative and ion-ion recombination ($O^+ + e \rightarrow O^*$; $O^+ + O^- \rightarrow O + O^*$) and from dissociative recombination ($O_2^+ + e \rightarrow O + O^*$). Key features arising from the O^+ recombination processes are OI 1356 A and OI 1304 A. The single useful feature from O_2^+ recombination is OI 6300 A (for nadir viewing conditions). We may relate their intensities respectively to the n_e maximum N_mF_2 and its location h_mF_2 by

$$\sqrt{4\pi I_{1356}} = g_1(N_mF_2)$$

and

$$\frac{\sqrt{4\pi I_{1356}}}{4\pi I_{6300}} = g_2(h_mF_2)$$

where $4\pi I$ is the column emission rate and g_1 and g_2 are functions dependent on the assumed shape of n_e and the chemistry (Tinsley and Bittencourt, 1975 and Chandra et al., 1975). Figure 1a and 1b show the important functional dependences within these equations. Here the shape of n_e is

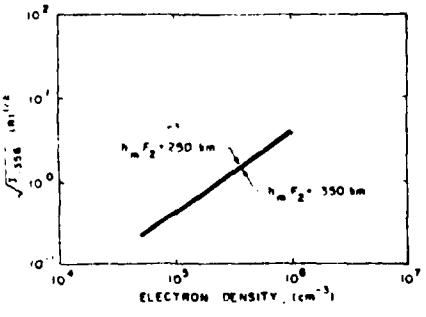

Figure 1a. The dependence of 1356 A intensity on the peak electron density, N_mF_2. The ordinate is the square root of the intensity. It is a linear function of N_mF_2 and has only a weak dependence on h_mF_2

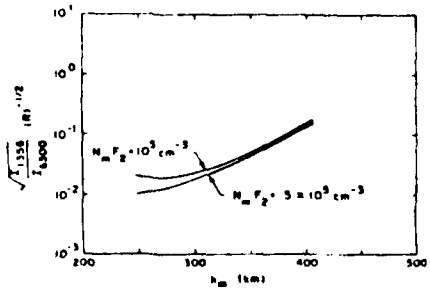

Figure 1b. The dependence of 6300 A intensity on the height of the electron density peak, h_mF_2. The ordinate is the ratio of the square root of the 1356 A intensity to the 6300 A intensity

given by a modified Chapman function, which generally characterizes n_e reasonably well over the altitude range containing most of the total electron content. The square root of the 1356 A intensity is very nearly proportional to N_mF_2 and insensitive to h_mF_2. The ratio of the square root of the 1356 A intensity to the 6300 A intensity is a sensitive function of h_mF_2 but nearly independent of N_mF_2. Note the log like dependence of $\sqrt{4\pi I_{1356}}/4\pi I_{6300}$ in Figure 1b. This dependence, especially for $h_mF_2 \sim 300$ km, is favorable for determining h_mF_2 even in the presence of likely levels of uncertainty in the intensities.

4. NIGHTTIME ELECTRON DENSITY AND EMISSION CHARACTERISTICS

The midlatitude ionosphere undergoes diurnal, seasonal, and solar cycle variations as well as irregular changes associated with magnetic storms. Latitudinal variations are relatively modest at middle latitudes, but geomagnetic disturbance effects are strongest in the high latitude region. The normal extremes in peak density are 5×10^4 cm^{-3} (usually just before dawn) and 10^6 cm^{-3} (usually just after sunset), with occasional excursions outside this range due to geomagnetic disturbances and solar activity. The height of the peak is almost always above 250 km during the night and commonly rises to 300-350 km near midnight (500 km at the equator).

Because the D, E, and F_1 regions are composed of molecular ions, they tend to disappear at night due to rapid recombination. A small E layer (generally less than 10^4 cm^{-3}) is maintained throughout the night by scattered EUV radiation (Bauer, 1973; Schunk and Nagy, 1980). The F_2 region is dominated by O^+ and is maintained by downward diffusion of O^+ from higher altitudes. These O^+ ions are lost due to charge exchange with molecular species below the peak. The peak occurs near the altitude where the time scale for vertical transport equals the chemical time scale (Bauer, 1973). Because vertical transport is significantly influenced by neutral winds, the variability of the F_2 peak is closely related to variability in the thermospheric circulation. For example, equatorward directed winds blow the plasma up along field lines. This produces not only a higher altitude for the F_2 peak but also a greater density at the peak because chemical loss rates decrease rapidly with increasing height due to decreasing neutral density (see, e.g. Evans, 1975; Strobel and McElroy, 1970). The reverse, of course, applies for poleward winds.

Of the emission features which can be used for ionospheric monitoring, two important ones are the atomic oxygen lines with wavelengths of 6300 A and 1356 A. We have developed a computer code which calculates the intensity of these features as they would be observed by a high altitude satellite. This code is based on the model described by Tinsley and Bittencourt (1975) and Chandra et al. (1975). Using the diurnal and seasonal variations displayed in Figure 2 and this computer code, we have calculated the corresponding variation in the emission features. The intensities as a function of local time are shown in Figure 3. Note that while the 6300 A intensity generally lies between 10 and 100 Rayleighs, the 1356 A intensity lies between 0.05 and 2 Rayleighs. The low end of the range of 1356 A intensities is reached sometime during the night regardless of season. These values are the worst case, solar minimum, and will generally be larger at solar maximum.

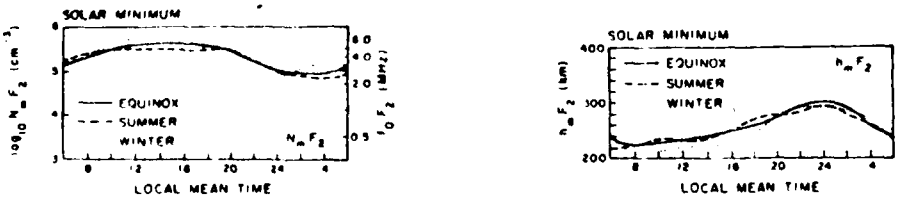

Figure 2. Comparison of the diurnal variation of the peak electron density (N_mF_2) and height of the peak (h_mF_2) over Millstone Hill for summer, winter, and equinox near solar minimum (After Evans, 1967.)

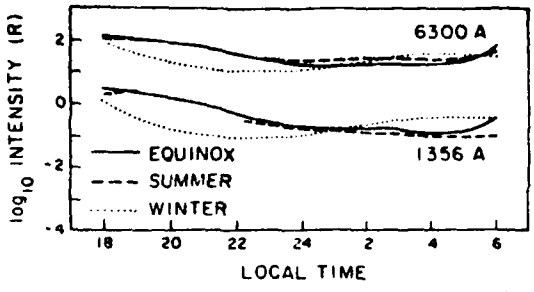

Figure 3. Local time variations of 6300 A and 1356 A emissions for summer, winter, and equinox conditions. The calculated intensities are based on the electron density information in Figure 2.

A representative latitudinal variation of the 6300 A and 1356 A intensities is shown in Figure 4. These were calculated using a representative ionospheric variation shown in Figure 5. (This figure is a synthesis of data from the Alouette and ISIS satellites as reported by Muldrew, 1965, Nelms and Lockwood, 1967, and Chan and Colin, 1969). For this particular example, the 6300 A intensity falls between 1 and 10 Rayleighs while the 1356 A intensity has about the same range as in Figure 3. Thus a conservatively designed optical system intended for use as an ionospheric monitor must be capable of detecting as little as 1 Rayleigh of 6300 and 0.05 Rayleigh of 1356 A.

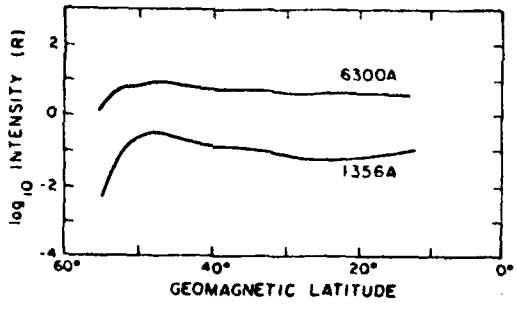

Figure 4. Latitudinal variation of 6300 and 1356 A emissions for conditions representative of the post-midnight, winter ionosphere near solar maximum. The calculated intensities are based on the electron densities of Figure 5.

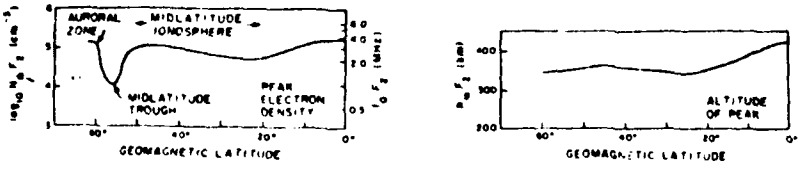

Figure 5. Latitudinal variation of peak electron density (N_mF_2) and the height of the peak (h_mF_2). The plot is representative of ionospheric conditions after midnight, in winter, and near solar maximum. (See text for sources.)

5. FACTORS WHICH AFFECT THE ACCURACY OF THE DEDUCED IONOSPHERIC PARAMETERS

The problem of monitoring the ionosphere using optical emissions may be separated into two parts: (1) the measurement of the intensities of the optical emissions and (2) the calculation of the electron density profile from the measured intensities. The accuracy of the final result depends on the uncertainties associated with each step. The uncertainty of the first step is controlled by the characteristics of the measuring instrument, the characteristics of the emissions being measured, and the statistical properties of the measurement process. The accuracy of the second step depends on the accuracy of the model used to connect optical intensities to the electron density as well as on the uncertainties of the parameters used in that model.

The characteristics of the instrument, such as sensitivity, affect the accuracy of the measurement because they are imperfectly known. The major contributor to uncertainty is the instrument sensitivity which is determined by calibration with a standard light source. The geometric factors (aperture and field of view) usually contribute very little uncertainty. For example, Huffman et al. (1980) cite uncertainties of 2%, 3%, and 7-12% for aperture, field of view, and sensitivity of the optical instruments on the S3-4 spacecraft.

The measurement process consists of counting photons with an efficiency determined by the instrument sensitivity. The number of counts recorded during a given integration time has a statistical uncertainty which is inversely proportional to its own square root. Increasing the integration time reduces this uncertainty. In addition, the instrument has a dark counting rate caused by energetic particles in the space environment. The dark count must be subtracted from the nominal count and has its own statistical uncertainty. The previously cited S3-4 instruments had dark count rates of 0.5-0.8 counts sec^{-1} in the laboratory, 4-7 counts sec^{-1} in space at low and middle latitudes, and 25-50 counts sec^{-1} in the polar regions.

In the ultraviolet part of the spectrum, extraneous background emissions are usually not a problem. (See below for exceptions.) In the visible part of the spectrum, however, there are normally two sources of background emissions. (Again, see below for exceptinnal cases.) The first of these is due to extraneous airglow features which are unrelated to ionospheric processes. For the OI 6300 A line, this means one or more lines of the OH (9-3) band. The other source of background is light reflected from the ground and clouds or scattered by aerosols in the lower atmosphere. This includes the continuum from astronomical sources (moon, stars, and the zodiacal light), the OH lines, and the OI 6300 A line itself. The OH contamination can be monitored by observing nearby, isolated OH lines. The reflected astronomical light can also be monitored by observing at nearby wavelengths between airglow features. Furthermore, if the incident intensity of the astronomical source is known, the effective albedo can be calculated and used to subtract the reflected OI 6300 A intensity.

During magnetic storms, energetic oxygen atoms and ions are precipitated at midlatitudes from the ring current (Rohrbaugh et al., 1983). This precipitation can stimulate as much as 20 kR of OI 6300 A and 100 R of OI 7774 A (equivalent to 140 R of OI 1356 A). This is sufficient to completely obscure the contribution from the ambient ionosphere. Torr et al. (1976) reported that even under magnetically quiet conditions, there are times when energetic electrons and protons precipitate at midlatitudes. Using the electron spectra which they reported, we have calculated intensities of 1.5 R of OI 6300 A and 0.04 R of OI 1356 A. These are comparable to the minimum intensities which we expect to see from the nighttime ionosphere. Huffman et al. (1980) observed N_2 LBH band emission at midlatitudes, most frequently during northern summer. The cause of this emission is unknown (Meier and Conway, 1983) and it tends to obscure both the OI 1356 A and the OI 1304 A lines. Note that none of these events causes contamination of the OI 911 A ionization continuum. Although it is only half as bright as OI 1356 A, it could also be used as a monitor of electron density.

Once the relevant intensities (such as OI 1356 A and OI 6300 A) have been determined, they may be used to calculate the peak electron density and its height using the method described in Section 3. In addition to the uncertainties associated with the intensities, there are uncertainties introduced by the calculation method itself. First, the method requires values for a number of parameters which are not known exactly. These include exospheric temperature, neutral densities, and various reaction rates. Second, the method depends on an assumed shape for the electron density profile (the modified Chapman function). Under most circumstances, this shape will differ from the true profile although it generally reproduces the peak quite well. (See Section 6 for an example.)

In order to assess the feasibility of using optical emissions to monitor the nighttime ionosphere, we have analyzed the capabilities of the S3-4 photometer with its 1340 A filter (Huffman et al., 1980). Because the full width at half maximum of this filter is 151 A, the photometer will measure both OI 1304 A and OI 1356 A. Because the OI 1304 A line is subject to multiple scattering, there is greater uncertainty in relating its intensity to electron density than there is for OI 1356 A. For a given 1356 A intensity, we have estimated the 1304 A contribution to the photometer signal using the multiple scattering analysis of Strickland and Anderson (1977). The uncertainty associated with this estimate has not been included in our current analysis. Taking into account all other sources of uncertainty (calibration, geometric factors, counting statistics, and dark count) we have calculated the uncertainty in the measured intensity (1304 A and 1356 A) as a function of integration time for several values of the OI 1356 A intensity. We have done the same thing for peak electron density, taking into account uncertainties in model parameters. These results are shown in Figure 6. We did not take into account the error caused by assuming a Chapman layer shape for the electron density profile. It is clear that this photometer is capable of observing even the lowest expected intensity of OI 1356 A with reasonable integration times.

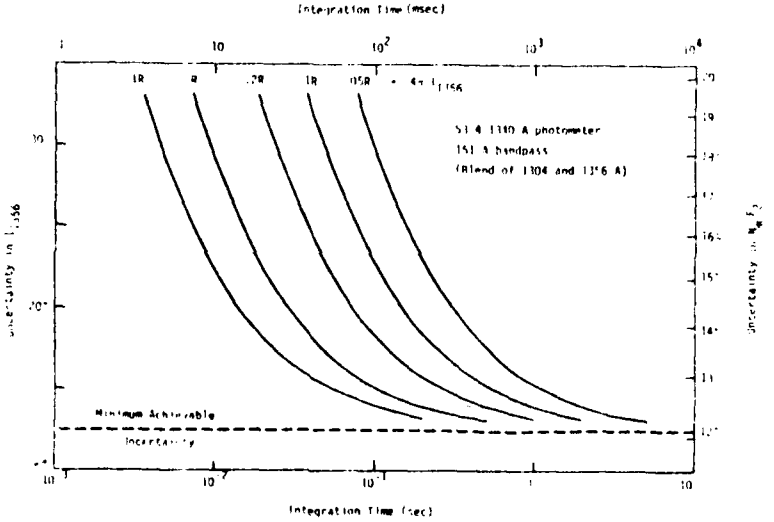

Figure 6. Uncertainties in $4\pi I_{1356}$ and $N_m F_2$ as functions of integration time for various values of the OI 1356 A intensity. The 1340 A photometer on the S3-4 satellite (Huffman et al., 1980) was used as a model for this analysis.

No 6300 A photometer designed to allow accurate subtraction of the background has ever been flown on a spacecraft. We believe that a state-of-the-art tilting filter photometer could do the job. However, our analysis of such a hypothetical system indicates that under the least favorable conditions (full moon, fresh snow, and 1 R of OI 6300 A), integration times of 60 seconds may be required. For a system located at 800 km altitude, this means that the spatial resolution is 3.6° of latitude. (Note, however, that this emission intensity is required only to obtain the height of the peak. The peak density can be determined on a much finer scale from the 1356 A intensity alone.) To prove the feasibility of this system, a specially designed instrument needs to be flown so that both instrument performance and the background problem can be properly assessed.

6. APPLICATION OF MODEL UNDER STRONGLY DYNAMICAL CONDITIONS

The contour plots of Figure 7 illustrate a major challenge to any ab-initio modeled n_e calculation: a common major nighttime transport event. During summer, the lower mid-latitudes show significant decreases in the height and magnitude of n_e on many but not all nights near midnight. The contour plots for the three nights of data shown in Figure 7 are illustrative of the normal night-to-night variability. This variability leads to departures of n_e from state-of-the-art models that can be a factor of 5-10! Using the observed n_e at 0100 and 0230 local time on 25 June, we have calculated the intensities of OI 1356 A and OI 6300 A. Then, using the algorithm of Tinsley and Bittencourt (1975), we calculated n_e corresponding to those intensities. (In this algorithm the shape of ne is assumed to be a modified Chapman function.) The inferred n_e's are compared to the observed n_e in Figure 8. In contrast to conventional models that have been in error by about a factor of 8, our model (based on optical emission lines) agrees within about 20%, a striking improvement. Note that this simulation does not include the effects of instrumental uncertainties or uncertainties in model parameters.

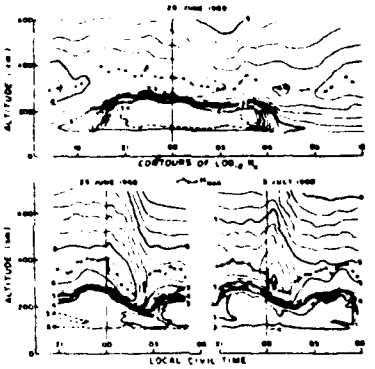

Figure 7. Contours in $\log_{10}$ of electron concentrations (electrons cm^{-3}), on an altitude versus local time grid, showing patterns of behavior in the nighttime mid-latitude ionosphere over Arecibo at 18.3 N geographic (29 N magnetic) latitude. Equatorward neutral winds are important in maintaining the nighttime ionosphere, as in the upper half of the figure. Transient poleward wind components of unknown origin generally sweep across the entire mid-latitude sector of the globe, manifested here by rapid order-of-magnitude drops in topside plasma concentrations and transient bottomside increases of two to three orders of magnitude (from Hanson and Carlson, 1977).

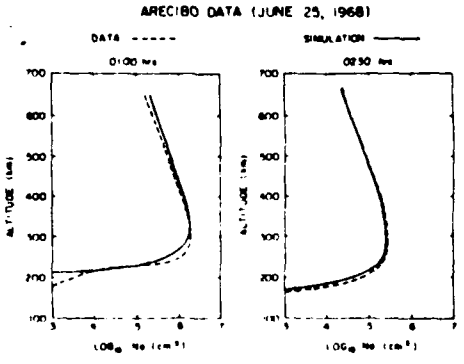

Figure 8. Calculated and observed n_e at 0100 and at 0230 local time on 25 June 1968. The observed n_e comes from Figure 7. The calculated n_e is based on 1356 A and 6300 A intensities derived from the observed n_e.

7. THE NIGHTTIME AURORAL IONOSPHERE

Auroral UV spectra can exhibit dramatic differences from one to another because of 1) composition change with altitude, time, and location and 2) O_2 pure absorption with its strong variation across the UV region. An extreme example of spectral variation may be seen in EUV data published by Paresce et al. (1981). Spectra are shown for a day and a night aurora. The incident electron spectrum is much softer for the day aurora and leads to preferential excitation of O compared to N_2. The result is a spectrum stronger in O and O^+ lines and weaker in N_2, N, and N^+ compared to a night auroral EUV spectrum. These spectral changes convey information on the incident electron spectrum and atmospheric composition as already noted earlier. Strickland et al. (1983) discuss in some detail the connection between these quantities and UV spectral changes as well as the connection with n_e. Here, we will limit our discussion to spectral variability for nadir viewing from satellite altitudes.

Figure 9 shows two synthetic spectra between 1000 and 1800 A for incident electron spectra given by .5 and 4 keV Maxwellian distributions. Each distribution is isotropic in the incidence plane over the downward hemisphere and contains 1 erg/cm^2-s. The original spectra have been smoothed to give a resolution of 30 A. The spectra displayed are partial spectra. They do not include, e.g., the optically thick features OI 1304 A, HI 1216 A, and OI 1027 A. For the given resolution, a number of features are blended. Twenty LBH bands are present even though fewer peaks are exhibited in their spectral region. The NI and NII features shown arise from electron impact on N_2 rather than on N. The original intensities were calculated using the transport algorithm of Strickland et al. (1976) with a Jacchia (1977) model atmosphere having an exospheric temperature of 1000 K.

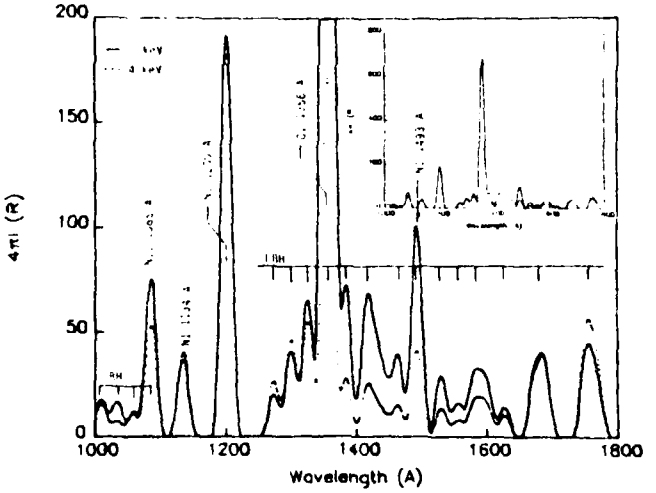

Figure 9. Calculated nadir viewing UV spectra for incident electron spectra given by .5 and 4 keV Maxwellians. The insert shows the same spectra on an enlarged vertical scale.

The exhibited differences at selected wavelengths due to changes in the hardness of the electron source have been discussed by Strickland et al. (1983) and here we will be brief. The 1356 A feature (OI 1356 A and LBH 1354 A) is particularly sensitive to the electron spectrum and serves as a useful indicator of this quantity provided the O density is known. The LBH spectrum is also shown to exhibit measurable change for the electron spectra considered. For the 4 keV case, this spectrum becomes depressed between 1350 and 1600 A due to O_2 absorption.

Ultimately we wish to determine how accurately n_e in the E and lower F regions can be specified from spectra such as those shown in Figure 9. We have the theoretical relationship between these quantities for fixed conditions which include the neutral atmosphere (N and NO as well as N_2, O_2, and O) and duration of the precipitation. Preliminary analysis has been carried out to assign error bars to the deduced n_e for some of the uncertain physical parameters. More work is required before reporting these results.

8. THE DAYTIME IONOSPHERE

Noticable changes in UV spectral shape were observed in the auroral results in the previous section. This will not occur in dayglow UV spectra [over modest changes in the solar zenith angle (S/A)] since the altitude profiles of volumes emission are relatively fixed compared to those under changing auroral conditions. What will change is overall brightness of dayglow UV spectra as solar activity changes. An exception does occur if the O density profile varies relative to that of N_2. In this situation, features such as OI 1356 A will also vary relative to such features as LBH 1383 A.

Figure 10 shows spectra similar to those in Figure 9 except for the dayglow. The intensities were calculated with the model of Strickland and Meier (1982) using a Jacchia (1971) model atmosphere with an exospheric temperature of 1000 K. The solar zenith angle is 60°. The applied solar EUV spectra come from Torr et al (1979). Below 190 A, we use the results of Donnelly and Pope (1973) which were applied unchanged to the cases considered.

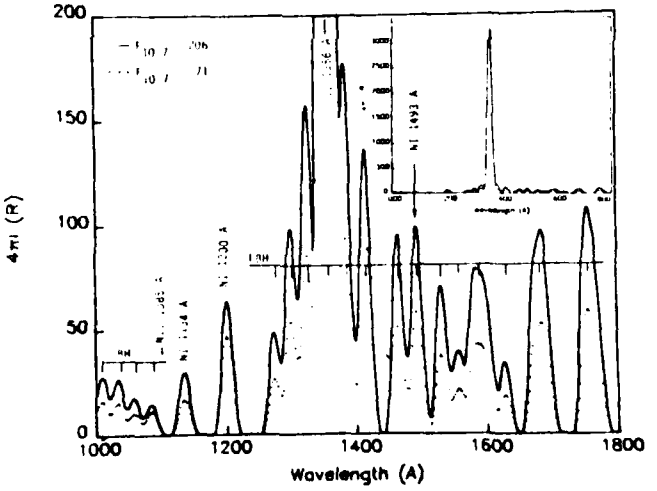

Figure 10. Similar to Figure 9 except for the dayglow.

The Torr et al. solar spectra identified by $F_{10.7}$ = 206 and 71 were used to generate the two spectra in Figure 10. The results are intended to reflect conditions under high and low solar activity. The differences are clearly measureable and suggest that monitoring of this spectral region will be useful for determining the overall energy content of that part of the solar spectrum responsible for maintaining the ionosphere. This region will also be useful for determining the amount of O present and with these two pieces of information, we should be able to specify n_e reasonable well (say 30%) in the E and lower F regions. We are attempting to better quantify this statement through searches for candidate optical and n_e data to which our predictions will be compared.

Anderson, D.E., Jr., R.R. Meier, and C.S. Weller, Observations of Far and Extreme Ultraviolet OI Emissions in Tropical Ionosphere, Planet. Space Sci., 24, 945, 1976.

Barth, C.A., and S. Schaffner, OGO-4 Spectrometer Measurements of the Tropical Ultraviolet Airglow, J. Geophys. Res., 75, 4299, 1970.

Bauer, S.J., Physics of Planetary Ionospheres, Springer, New York, 183, 1973.

Chakrabarti, S., F., Parasce, S. Bowyer, R. Kimble and S. Kumar, The Extreme Ultraviolet Day Airglow, J. Geophys. Res., 88, 4894, 1983.

Chan, K.L. and L. Colin, Global Electron Density Distributions From Topside Soundings, Proc. IEEE, 57, 990, 1969.

Chandra, S.E., E.I. Reed, R.R. Meier, C.B. Opal, and G.T. Hicks, Remote Sensing of the Ionospheric F-Layer by use of OI 6300 A and OI 1356 A Observations, J. Geophys. Res., 80, 2327, 1975.

Donnelly, R.F. and J.H. Pope, The 1-3000 A Solar Flux for a Moderate Level of Solar Activity for use in Modeling the Ionosphere and Upper Atmosphere, Tech. Rep. ERL 276-SEL 25, NOAA, Boulder, Colo., 1973.

Evans, J.V., Midlatitude F-Region Densities and Temperatures at Sunspot Minimum, Planet. Space Sci., 15, 1387, 1967.

Evans, J.V., A Review of F-Region Dynamics, Rev. Geophys. Space Phys., 13, 887, 1975.

Gentieu, E.P., P.D. Feldman, and R.R. Meier, Spectroscopy of the Extreme Ultraviolet Dayglow at 6.5 A Resolution: Atomic and Ionic Emissions Between 530 and 1240 A, Geophys. Res. Lett.,6, 325, 1979.

Hanson, W.B. and H.C. Carlson, The Ionosphere, from the Upper Atmosphere and Magnetosphere, National Academy of Sciences, Washington, D.C. 1977.

Huffman, R.E., F.J. LeBlanc, J.C. Larrabee, and D.F. Paulsen, Satellite Vacuum Ultraviolet Airglow and Auroral Observations, J. Geophys. Res., 85, 2201, 1980.

Jacchia, L.G., Revised Static Models of the Thermosphere and Exosphere with Empirical Temperature Profiles, Smithsonian Astrophysical Observatory Special Report 332, 1971.

Jacchia, L.G., Thermospheric Temperature, Density, and Composition: New Models, Smithsonian Astrophysical Observatory Special Report 375, 1977.

Meier, R.R. and D.E. Anderson, Jr., Determination of Atmospheric Composition and Temperature from the UV Airglow, Planet. Space Sci., 31, 967, 1983.

Meier, R.R. and R.R. Conway, On the N_2 Lyman-Birge-Hopefield Band Nightglow, J. Geophys. Res., 88, 4929, 1383.

Meier, R.R. and C.B. Opal, Tropical UV Arcs: Comparison of Brightness with f_0F_2, J. Geophys. Res., 78, 3189, 1973.

Meier, R.R., D.J. Strickland, P.D. Feldman, and E.P. Gentieu, The Ultraviolet Dayglow, 1. Far UV Emissions of N and N_2, J. Geophys. Res., 85, 2177, 1980.

Meier, R.R., R.R. Conway, P.D. Feldman, D.J. Strickland, and E.P. Gentieu, Analysis of Nitrogen and Oxygen Far Ultraviolet Auroral Emission, J. Geophys. Res., 87, 2444, 1982.

Muldrew, D.B., F-Layer Ionization Troughs Deduced from Alouette Data, J. Geophys. Res., 70, 2635, 1965.

Nelms, G.L. and G.E.K. Lockwood, Early Results From the Topside Sounder in the Alouette II Satellite, Space Research VII, 604, 1967.

Parasce, F. S. Chakrabarti, S. Bowyer, and R. Kimable, The Extreme Ultraviolet Spectrum of Dayside and Nightside Aurora: 800-1400 A, J. Geophys. Res., 88, 1005, 1983.

DTIC

FILMED

4-86

END